

Electron Cooling studies for RHIC-II

- I.A.1 RHIC-II parameters**
 - I.A.1.1 Expected performance for heavy ions and protons**
 - I.A.1.2 Non-magnetized vs magnetized cooling**
 - I.A.1.3 Parameters of electron cooler**
 - I.A.1.4 Suppression of recombination with undulators**
- I.A.2 Friction force description**
 - I.A.2.1 Non-magnetized friction force calculation**
 - I.A.2.2 Comparison with direct numeric simulation**
 - I.A.2.3 Comparison with experimental data**
 - I.A.2.4 Friction force in the presence of an undulator field**
- I.A.3 Intrabeam scattering**
 - I.A.3.1 General models**
 - I.A.3.2 IBS in RHIC: experiments vs theory**
 - I.A.3.3 IBS for ion beam distribution under electron cooling**
- I.A.4 Recombination**
 - I.A.4.1 Numerical algorithm**
 - I.A.4.2 Experimental measurements and theory**
 - I.A.4.3 Parameters of undulator**
- I.A.5 Detailed calculation of cooling dynamics**
 - I.A.5.1 Baseline parameters**
 - I.A.5.2 Detailed evolution of beam distribution**
 - I.A.5.3 Requirement on transverse emittance of electron beam**
 - I.A.5.4 Requirement on longitudinal momentum spread of electron beam**
 - I.A.5.5 Cooling with realistic 6-D distribution of electrons**
 - I.A.5.6 Cooling optimization**
 - I.A.5.7 Cooling performance with and without recombination suppression**
- I.A.6 Scenarios of cooling at RHIC-II: heavy ions**
- I.A.7 Scenarios of cooling at RHIC-II: protons**
- I.A.8 Luminosity limitations under cooling**
 - I.A.8.1 Incoherent beam-beam effects**
 - I.A.8.2 Coherent beam-beam effects**
 - I.A.8.3 Non-linear effects and beam-beam limit**
 - I.A.8.4 Beam-beam simulations for ion beam under cooling**
- I.A.9 Effects on electron beam**
- I.A.10 Effects of electron beam on ion beam dynamics**
 - I.A.10.1 Tune shifts**
 - I.A.10.2 Coherent ion-electron interactions**
 - I.A.10.3 Collective instabilities for ion distribution under cooling**
 - I.A.10.4 Effects of cooling on polarization**
- I.A.11 References**

I.A.1 RHIC-II parameters

This is a DRAFT of a working document.

In this document we freely use material prepared for BNL by our collaborators. In particular, by the Dubna group as part of our collaboration on the development of the BETACOOOL code [1], by the Tech-X group as part of our collaboration on numerical study of the friction force with the VORPAL [2] code, and by the Fermilab electron cooling group as part of our collaboration on experimental study of the non-magnetized friction force [3].

I.A.1.1. Expected performance for heavy ions and protons

Present performance of the RHIC collider with heavy ions is limited by the process of Intra-Beam Scattering (IBS) within the beam. To achieve required luminosities for the future upgrade of the RHIC complex (known as RHIC-II) an Electron cooling system was proposed [4].

The baseline of the heavy-ion program for RHIC is operation with Au ions at total energy per beam of 100 GeV/n. For such an operation, the electron cooling should compensate IBS and provide about factor of 10 increase in average luminosity per store.

For RHIC operation with the protons, the electron cooling should assist in obtaining slightly low transverse and longitudinal emittances or prevent their significant increase due to IBS. Although, IBS is not as severe for protons as for heavy ions, a proposed increase in proton intensity for RHIC-II upgrade makes IBS one of the dominant effects as well.

Table I.A.1.1. Performance for RHIC-II

Gold at 100 GeV/n per beam	w/o e-cooling	With e-cooling
Emittance (95% norm.) [$\pi \mu\text{m}$]	15 \rightarrow 30 (depending on the length of the store)	15 \rightarrow 12
β -function in IR [m]	1.0	0.5
Number of bunches	112	112
Bunch population [10^9]	1	1
Peak luminosity [$10^{26} \text{ cm}^2 \text{ s}^{-1}$]	30	90
Average store luminosity [10^{26}]	8-10	70
Protons at 250 GeV	w/o e-cooling	with e-cooling
Emittance (95% norm.) [$\pi \mu\text{m}$]	20	12
β -function	1.0	0.5
Number of bunches	112	112
Bunch population [10^{11}]	2	2
Average store luminosity [10^{30}]	150	500

Without cooling:

For present operation with Au ions:

- a) There is a significant emittance increase due to IBS which results in the luminosity loss. This is shown, for example, in Fig. I.A.1.1 (Run-2004 experimental data).
- b) In addition, there is a significant growth of the bunch length which leads to particle loss from the bucket. Also, with such a long bunch length only central portion of the longitudinal beam distribution can effectively contribute to counts in the detector which results in an additional loss of effective luminosity.

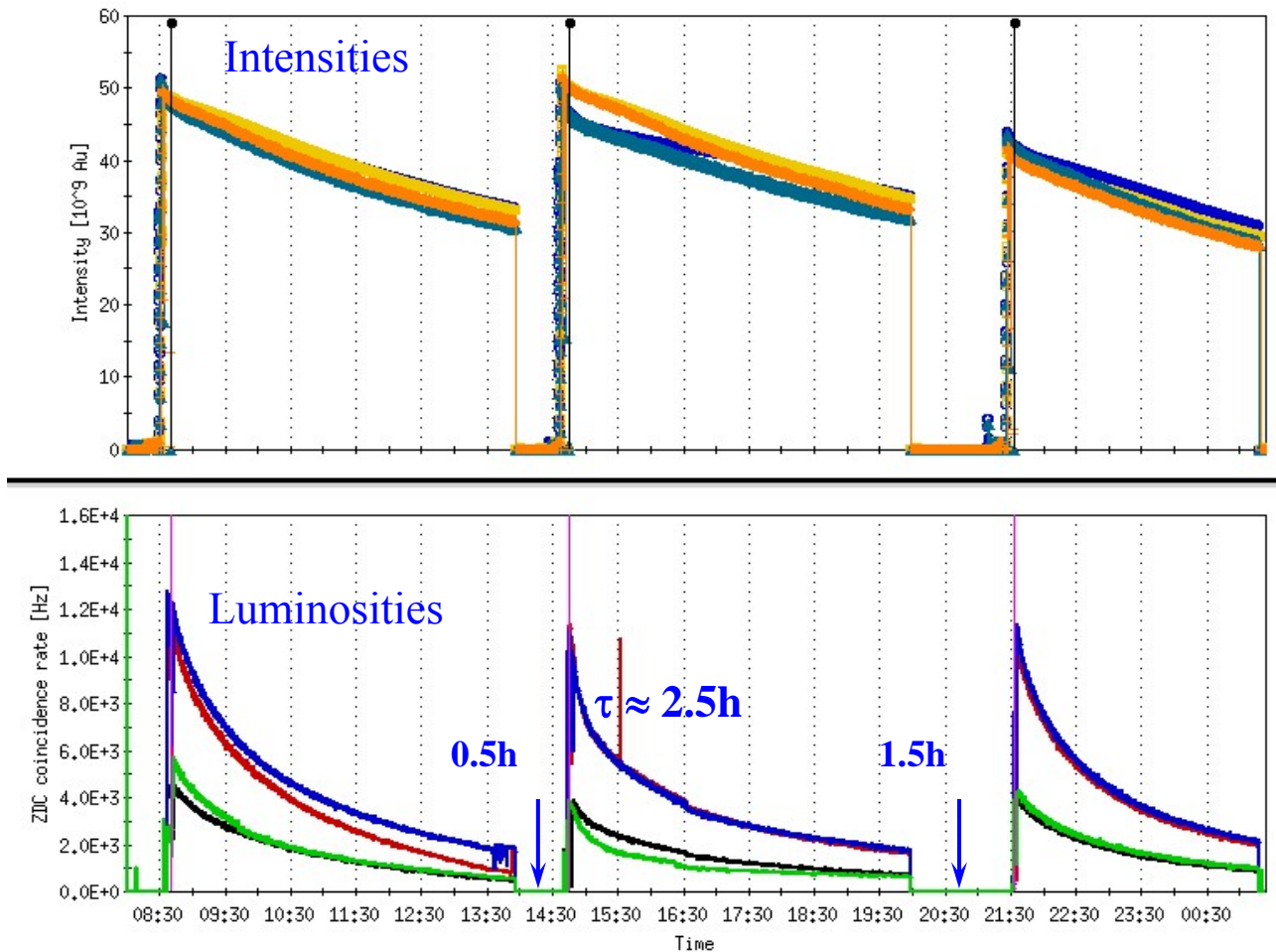


Fig. I.A.1.1 Run-2004 experiment with Au ions (40 bunches).

Note that for the enhanced luminosity of RHIC-II without cooling, the optimum length of the store is shorter than for typical RHIC stores, shown in Fig. I.A.1.1.

With cooling:

Electron cooling of Au ions at the total beam energy of 100 GeV/n will bring into reach the desired increase of the average luminosity for the RHIC upgrade, which is about factor of 40 larger than the original design value. For the RHIC-II upgrade, electron cooling can provide about factor of 7 increase in the luminosity of Au ions, as compared to the upgrade without cooling.

Figure 1.A.1.2 shows the luminosity for RHIC-II parameters (Table I.A.1.2) based on the present approach of the non-magnetized cooling. For present RHIC operation without electron cooling, β^* (the beta function at the IP) is limited to about one meter (or slightly less), because the emittance is increased by a factor of two due to IBS. Further reduction of β^* with such an increase of the emittance would lead to a significant angular spread and beam loss. On the other hand, keeping the rms emittance constant (by cooling), allows one to begin a store cycle with smaller values of β^* . This is taken into account in Fig. I.A.1.2, where $\beta^*=0.5$ and 1 m were used with and without electron cooling, respectively.

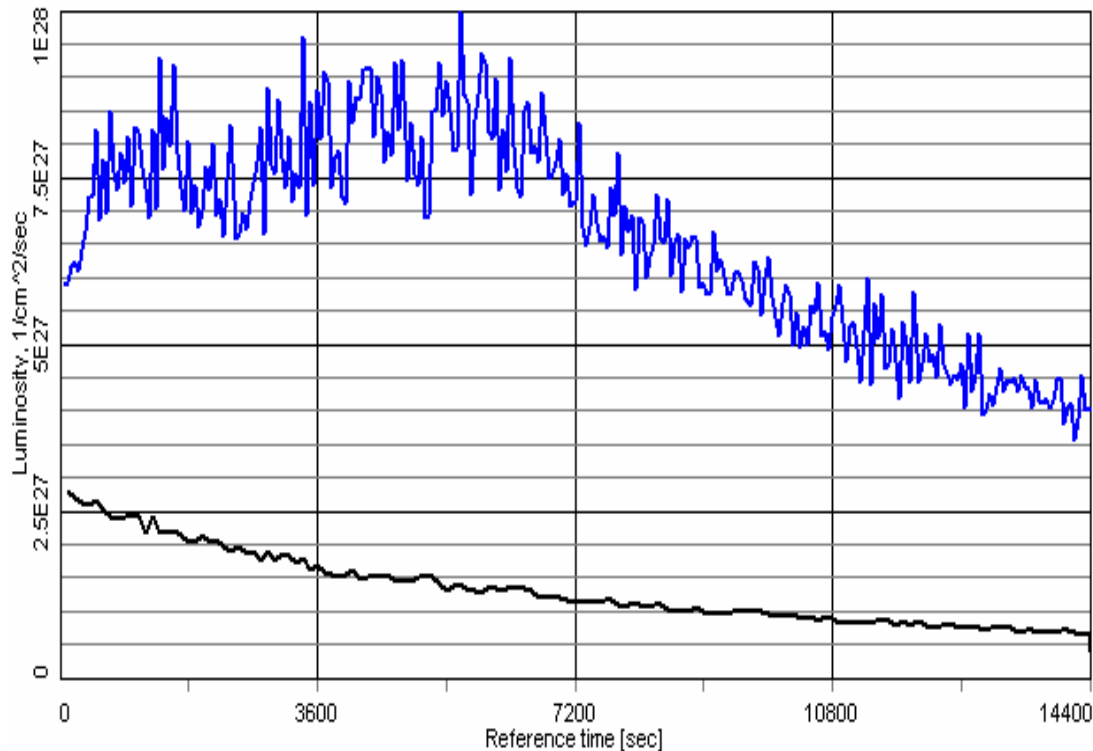


Fig. I.A.1.2: Simulated luminosity for the RHIC-II upgrade, with (blue top curve) and without (black bottom curve) electron cooling, taking $\beta^*=0.5$ m and 1 m, respectively.

The average luminosity with cooling in Fig. 1.A.1.2 (using parameters in Table I.A.1.2) is $\langle L \rangle = 7 \cdot 10^{27}$ [$\text{cm}^2 \text{sec}^{-1}$]. This number is a result of simulations based on the “modeled beam” approach which simulates detailed evolution of ions distribution. Simulations based on such a “detailed dynamics” predict larger average luminosity than a more simplified “rms dynamics” approach but the uncertainty of various algorithms and numerical effects becomes larger as well. All this is summarized in Section I.A.5.

I.A.1.2. Non-magnetized vs magnetized cooling

The traditional electron cooling system employed at any low-energy cooler is based on electron beam generated with an electrostatic electron gun in DC operating mode, immersed in a longitudinal magnetic field. The magnetic field is used for the transport of an electron beam through the cooling section from the gun to the collector. The magnetic field value is determined by condition of electron “magnetization” – radius of the electron Larmor rotation in the transverse plane has to be much less than the beam radius. The presence of a strong longitudinal magnetic field changes the collision kinetics significantly. The magnetic field limits transverse motion of the electrons. In the limit of a very strong magnetic field, the transverse degree of freedom does not take part in the energy exchange, because collisions are adiabatically slow relative to the Larmor oscillations. As a result, the efficiency of electron cooling is determined mainly by the longitudinal velocity spread of the electrons. Such type of cooling is typically referred to as a “magnetized cooling”. Magnetized cooling was found extremely useful technique in obtaining high-brightness hadron beams with extremely low longitudinal momentum spread [5].

However, if an rms velocity spread within electron beam is comparable or smaller than the spread within the ion beam and, and there is no requirement of getting ultra-cold ion state, the cooling can be done without the help of the strong external magnetic field. Such type of cooling is referred to as the “non-magnetized cooling”, although weak external field can be still employed, for example, to ensure focusing and alignment of electron and ion beams.

The first cooling system which is based on the “non-magnetized” approach was successfully constructed at FNAL Recycler ring. It is in operation since July 2005. The Recycler’s cooling system is also the cooler with the highest energy of the electrons presently in operation (4.3 MeV) [3].

Although extensive studies of the magnetized cooling approach for RHIC showed that such approach is feasible [4, 6] and would provide required luminosities for the RHIC-II, the baseline was recently changed to the non-magnetized one.

Electron cooling at RHIC using the non-magnetized electron beam significantly simplifies the cooler design. Generation and acceleration of the electron bunch without longitudinal magnetic field allows to reach a low value of the emittance for the electron beam in the cooling section. The cooling rate required for suppression of the Intra-Beam Scattering (IBS) can be achieved with a relatively small charge of the electron bunch ~ 5 nC ($3 \cdot 10^{10}$ electrons per bunch).

For cooling of Au ions in RHIC at the beam energy of 100 GeV/n, the kinetic energy of the electron beam has to be 54.3 MeV. Such a high-energy electron cooling system for RHIC is based on the Energy Recovery Linac (ERL) [7].

I.A.1.3. Parameters of electron cooler

Table I.A.1.2 summarizes parameters of typical beam of Au ions at the store energy of 100GeV/n and parameters of the proposed RHIC-II cooler.

Table I.A.1.2. Ion and electron beam parameters

Ion rms beam emittance normalized [$\pi \cdot \text{mm} \cdot \text{mrad}$]	2.5
Ion rms momentum spread	$5 \cdot 10^{-4}$
Number of ions per bunch	10^9
Ion beta functions in the cooling section [m]	400
Ion rms beam radius [mm]	3
Ion initial rms bunch length [cm]	20
Circumference of RHIC ring [m]	3833
Electron cooler length [m]	80
Electron rms beam emittance normalized [$\pi \cdot \text{mm} \cdot \text{mrad}$]	4
Electron rms momentum spread	$3 \cdot 10^{-4}$
Number of electrons per bunch	$3 \cdot 10^{10}$
Electron rms beam radius [mm]	4.3
Electron rms bunch length [cm]	1
Relativistic factor γ (ions, electrons)	107.35

Table I.A.1.3. Ion and electron beam rms velocities (PRF) corresponding to Table I.A.1.2:

Ion transverse rms velocity [m/s]	$2.5 \cdot 10^5$
Ion longitudinal rms velocity [m/s]	$1.5 \cdot 10^5$
Electron transverse rms velocity [m/s]	$2.8 \cdot 10^5$
Electron longitudinal rms velocity [m/s]	$9.0 \cdot 10^4$

I.A.1.4. Suppression of recombination with undulators

Non-magnetized cooling requires low temperature of the electrons in the cooling section. However, a general problem of such an approach is high recombination rate for low electron temperature [4].

Presently, suppression of the ion recombination for RHIC is considered using an undulator field in the cooling section [8, 9]. In the presence of an undulator field, trajectories of all electrons have the same coherent azimuth angle θ , determined by the undulator period λ and field value B at the axis:

$$\theta = \frac{eB\lambda}{2\pi pc}, \quad (\text{I.A.1.1})$$

where p is the electron momentum.

The recombination coefficient, determined via recombination cross section σ as

$$\alpha_r = \int (V_i - v_e) \sigma(V_i - v_e) f(v_e) d^3 v_e, \quad (\text{I.A.1.2})$$

has to be calculated taking into account the coherent transverse electron velocity. Therefore, one can expect sufficient suppression of the recombination without significant loss in the friction force (see Section I.A.2.4).

To provide an estimate of an undulator efficiency we use the BETACOOOL code with calculation of the friction force and recombination rates based on numerical evolution of the integrals over the electron velocity distribution. For an accurate estimate of the loss due to recombination one should take into account that the intensity of the ion beam is sharply decreasing due to beam-beam collisions with disintegration in the IP region. Such disintegration (burn-off) depends on the distribution function of the ion beam which one gets as a result of Intra-beam Scattering (IBS) and cooling. All together, these dynamics processes (IBS, cooling, burn-off, recombination) are included in BETACOOOL and provide an estimate of the loss due to the recombination.

I.A.2 Friction force description

I.A.2.1. Non-magnetized friction force calculation

In the particle rest frame (PRF) the friction force acting on the ion with a charge number Z passing through an electron beam of density n_e can be accurately evaluated by numerical integration of the following formula [10, 11]:

$$\vec{F} = -\frac{4\pi m_e e^4 Z^2}{m} \int \ln\left(\frac{\rho_{\max}}{\rho_{\min}}\right) \frac{\vec{V} - \vec{v}_e}{|\vec{V} - \vec{v}_e|^3} f(v_e) d^3 v_e, \quad (\text{I.A.2.1})$$

where e and m are the electron charge and mass, V and v_e are the ion and electron velocities respectively. The Coulomb logarithm $L_c = \ln \frac{\rho_{\max}}{\rho_{\min}}$ is kept under the integral because the minimal impact parameter depends on electron velocity:

$$\rho_{\min} = \frac{Ze^2}{m} \frac{1}{|\vec{V} - \vec{v}_e|^2}. \quad (\text{I.A.2.2})$$

At a given value of the ion velocity the maximum impact parameter is constant and determined by either the dynamic shielding radius or the ion time of flight through the electron cloud. Radius of the dynamic shielding sphere coincides with the Debye radius

$$\rho_D = \frac{\Delta_e}{\omega_p}, \quad (\text{I.A.2.3})$$

when the ion velocity is less than the electron velocity spread Δ_e . The plasma frequency ω_p is equal to

$$\omega_p = \sqrt{\frac{4\pi n_e e^2}{m}}. \quad (\text{I.A.2.4})$$

When the ion velocity is larger than the electron velocity spread, the shielding distance is given by:

$$\rho_{sh} = \frac{V}{\omega_p}. \quad (\text{I.A.2.5})$$

The formulae (I.A.2.3) and (I.A.2.5) can be combined together to have a smooth dependence of the shielding radius on the ion velocity:

$$\rho_{sh} = \frac{\sqrt{V^2 + \Delta_e^2}}{\omega_p}. \quad (\text{I.A.2.6})$$

In the case when the shielding sphere does not contain large number of electrons to compensate the ion charge (such a situation takes a place, for example, in the case of the magnetized electron beam at low longitudinal velocity spread) it has to be increased in accordance with the electron beam density and the ion charge. In the BETACOOOL program such a radius is estimated from the expression

$$n_e \rho^3 \sim 3Z. \quad (\text{I.A.2.7})$$

As a result, the maximum impact parameter is calculated as a minimum from three values:

$$\rho_{\max} = \min \left\{ \max \left(\rho_{sh}, \sqrt[3]{\frac{3Z}{n_e}}, V\tau \right) \right\}. \quad (\text{I.A.2.8})$$

The second term describes the distance, which the ion passes inside the electron beam. Here τ is the ion time of flight through the cooling section in the PRF:

$$\tau = \frac{l_{cool}}{\beta\gamma c}. \quad (\text{I.A.2.9})$$

In the case of an axial symmetry the electron distribution function can be written in the following form:

$$f(v_e) = \left(\frac{1}{2\pi} \right)^{3/2} \frac{1}{\Delta_{\perp}^2 \Delta_{\parallel}} \exp \left(-\frac{v_{\perp}^2}{2\Delta_{\perp}^2} - \frac{v_{\parallel}^2}{2\Delta_{\parallel}^2} \right), \quad (\text{I.A.2.10})$$

where Δ_{\perp} and Δ_{\parallel} are the electron rms velocity spreads in the transverse and longitudinal direction, respectively. The shielding cloud in this case has an ellipsoidal shape which can be approximated by the sphere with the radius, calculated using effective electron velocity spread:

$$\Delta_e^2 = \Delta_{\perp}^2 + \Delta_{\parallel}^2. \quad (\text{I.A.2.11})$$

The components of the friction force (I.A.2.1) can be evaluated in cylindrical co-ordinate system as follows [1]:

$$\begin{aligned}
F_{\perp} &= -\sqrt{\frac{2}{\pi}} \frac{Z^2 e^4 n_e}{m \Delta_{\perp}^2 \Delta_{\parallel}} \int_0^{\infty} \int_{-\infty}^{\infty} \int_0^{2\pi} \ln\left(\frac{\rho_{\max}}{\rho_{\min}}\right) \frac{(V_{\perp} - v_{\perp} \cos \varphi) \exp\left(-\frac{v_{\perp}^2}{2\Delta_{\perp}^2} - \frac{v_{\parallel}^2}{2\Delta_{\parallel}^2}\right)}{\left((V_{\parallel} - v_{\parallel})^2 + (V_{\perp} - v_{\perp} \cos \varphi)^2 + v_{\perp}^2 \sin^2 \varphi\right)^{3/2}} v_{\perp} d\varphi dv_{\parallel} dv_{\perp}, \\
F_{\parallel} &= -\sqrt{\frac{2}{\pi}} \frac{Z^2 e^4 n_e}{m \Delta_{\perp}^2 \Delta_{\parallel}} \int_0^{\infty} \int_{-\infty}^{\infty} \int_0^{2\pi} \ln\left(\frac{\rho_{\max}}{\rho_{\min}}\right) \frac{(V_{\parallel} - v_{\parallel}) \exp\left(-\frac{v_{\perp}^2}{2\Delta_{\perp}^2} - \frac{v_{\parallel}^2}{2\Delta_{\parallel}^2}\right)}{\left((V_{\parallel} - v_{\parallel})^2 + (V_{\perp} - v_{\perp} \cos \varphi)^2 + v_{\perp}^2 \sin^2 \varphi\right)^{3/2}} v_{\perp} d\varphi dv_{\parallel} dv_{\perp}. \quad (\text{I.A.2.12})
\end{aligned}$$

Within an accuracy of about 2% the upper limit of the integrals over velocity components can be replaced from infinity to three corresponding rms values, and an integration over φ can be performed from 0 to π due to symmetry of the formulae. In this case the friction force components can be calculated as (such expressions are used in BETACOOl):

$$\begin{aligned}
F_{\perp} &= -\frac{4\pi Z^2 e^4 n_e}{m \cdot \text{Int}} \int_0^{3\Delta_{\perp}} \int_{-3\Delta_{\parallel}}^{3\Delta_{\parallel}} \int_0^{\pi} \ln\left(\frac{\rho_{\max}}{\rho_{\min}}\right) \frac{(V_{\perp} - v_{\perp} \cos \varphi) \exp\left(-\frac{v_{\perp}^2}{2\Delta_{\perp}^2} - \frac{v_{\parallel}^2}{2\Delta_{\parallel}^2}\right)}{\left((V_{\parallel} - v_{\parallel})^2 + (V_{\perp} - v_{\perp} \cos \varphi)^2 + v_{\perp}^2 \sin^2 \varphi\right)^{3/2}} v_{\perp} d\varphi dv_{\parallel} dv_{\perp}, \\
F_{\parallel} &= -\frac{4\pi Z^2 e^4 n_e}{m \cdot \text{Int}} \int_0^{3\Delta_{\perp}} \int_{-3\Delta_{\parallel}}^{3\Delta_{\parallel}} \int_0^{\pi} \ln\left(\frac{\rho_{\max}}{\rho_{\min}}\right) \frac{(V_{\parallel} - v_{\parallel}) \exp\left(-\frac{v_{\perp}^2}{2\Delta_{\perp}^2} - \frac{v_{\parallel}^2}{2\Delta_{\parallel}^2}\right)}{\left((V_{\parallel} - v_{\parallel})^2 + (V_{\perp} - v_{\perp} \cos \varphi)^2 + v_{\perp}^2 \sin^2 \varphi\right)^{3/2}} v_{\perp} d\varphi dv_{\parallel} dv_{\perp}, \quad (\text{I.A.2.13})
\end{aligned}$$

where the normalization factor is calculated in accordance with:

$$\text{Int} = \int_0^{3\Delta_{\perp}} \int_{-3\Delta_{\parallel}}^{3\Delta_{\parallel}} \int_0^{\pi} \exp\left(-\frac{v_{\perp}^2}{2\Delta_{\perp}^2} - \frac{v_{\parallel}^2}{2\Delta_{\parallel}^2}\right) v_{\perp} d\varphi dv_{\parallel} dv_{\perp}. \quad (\text{I.A.2.14})$$

The minimal impact parameter is the following function of the electron velocity components:

$$\rho_{\min} = \frac{Ze^2}{m_e} \frac{1}{(V_{\parallel} - v_{\parallel})^2 + (V_{\perp} - v_{\perp} \cos \varphi)^2 + v_{\perp}^2 \sin^2 \varphi}. \quad (\text{I.A.2.15})$$

When the Coulomb logarithm L_C is constant the two of the three integrals in Eq. (I.A.2.12) can be performed analytically and the friction force components can be written in accordance with Binney's formulae [12]. Such an algorithm significantly speeds up numerical evaluation of the friction force and is also included in the BETACOOl code.

I.A.2.2. Comparison with direct numeric simulation

The first step towards accurate calculation of cooling times is to use an accurate description of the cooling force. As for the previous case of the magnetized cooling, the VORPAL code [2] is being used to simulate from first principles the non-magnetized friction force and diffusion coefficients for the parameters of the RHIC cooler. For simulation of electron cooling problem, VORPAL uses molecular dynamics techniques and explicitly resolves close binary collisions to obtain the friction force and diffusion coefficient with a minimum of physical assumptions [13].

The latest version of the BETACOOOL code [1] includes numerical integration over the electron velocity distribution. This numerical evaluation of the force enables an accurate comparison with the VORPAL results, both for the magnetized and non-magnetized friction force with an anisotropic velocity distribution of the electrons. The results of such benchmarking are summarized in [14, 15].

For example, Fig. I.A.2.1 compares VORPAL data (dots with error bars) with the result of numerical integration based on Eq. (I.A.2.1) (solid red line), for the case of an anisotropic Maxwellian velocity distribution of the electrons given in Eq. (I.A.2.10), where $\Delta_{\perp}=4.2\cdot 10^5$ [m/s] and $\Delta_{\parallel}=1.0\cdot 10^5$ [m/s] ($Z=79$, $n_e=2\cdot 10^{15}$ m⁻³).

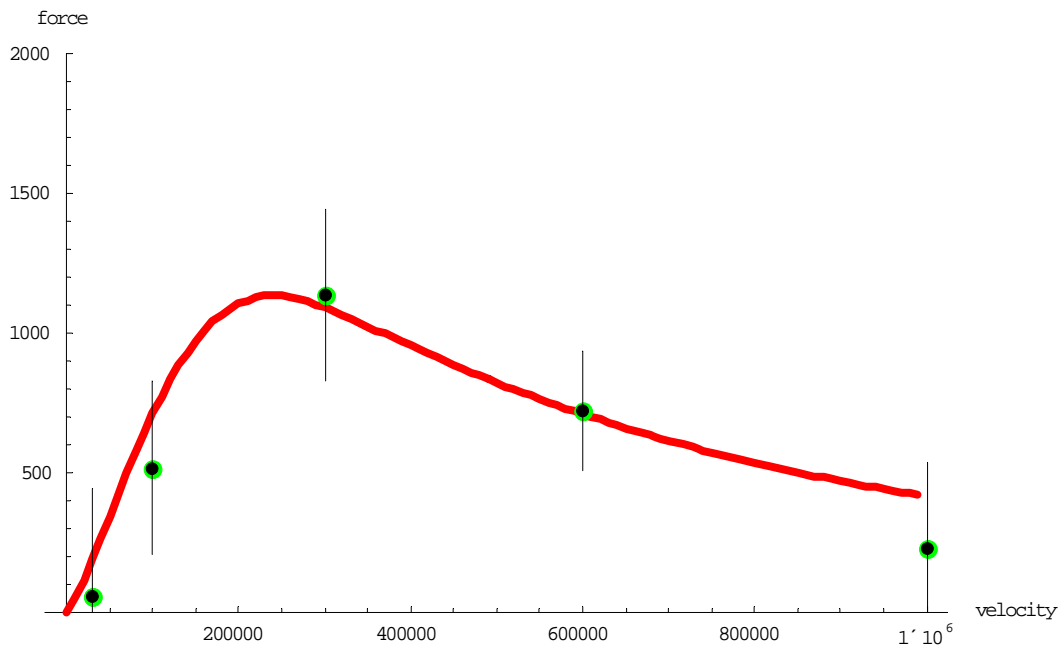


Fig. I.A.2.1. Non-magnetized friction force for an anisotropic electron velocity distribution. Force [eV/m] vs. ion velocity [m/s]: solid line (red) – numeric integration using BETACOOOL; points with errors bar (3 rms deviation shown)– simulations using VORPAL.

Simulations were done for other degrees of anisotropy of the electron velocity as well. We find agreement between VORPAL simulations and numeric integration satisfactory, and thus use the non-magnetized friction force in BETACOOOL (based on numerical evaluation of the integrals) in our simulations of the non-magnetized cooling.

I.A.2.3. Comparison with experimental data

In a typical low-energy electron cooling system strong longitudinal magnetic field is used for transportation of the electron beam. For decreased values of the magnetic field in the cooling section the beam quality is diminished and investigation of the non-magnetized regime of the electron cooling can not be provided with a well controlled conditions.

In July 2005 the Recycler cooling system was put into operation in Fermilab [3]. In Recycler's cooling system the longitudinal magnetic field in the cooling section is used only to preserve angular spread of the electrons θ at the level below 200 μ rad. The required longitudinal magnetic field value B is about 105 G that corresponds to electron rotation with Larmor radius

$$\rho_{\perp} = \frac{pc}{eB} \theta \approx 2.3 \cdot 10^{-4} m,$$

where $pc = 4.85$ MeV is the electron momentum. The cooling section length is $l_{cool}=20$ m which approximately corresponds to 2 steps of the Larmor helix. A maximum impact parameter for the maximum electron current of 500 mA is restricted by a time of flight through the cooling section and it is equal

$$\rho_{max} = \frac{l_{cool}}{\beta\gamma c} \approx 1.3 \cdot 10^{-3} m$$

With such parameters the contribution to the friction force is dominated by the non-magnetized collisions, which allows to refer to the cooling in Recycler as the “non-magnetized”.

To provide comparison between the results of the experimental studies at Recycler (FNAL) and numerical simulation within the BETACOOOL, several new algorithms were implemented in the code. A general method for the friction force measurements at the Recycler is Voltage Step method. Such a procedure was also explored within the BETACOOOL.

One of the features of the Recycler cooling system is strong dependence of the electron transverse velocity spread on the distance from the beam centre. This effect appears due to the beam envelope mismatch with the transport channel, and is called “envelope scalloping”. In the first approximation this effect can be presented as a linear increase of the velocity spread with radial co-ordinate:

$$\Delta_{\perp} = \frac{d\Delta_{\perp}}{dr} r, \quad (I.A.2.16)$$

where the velocity gradient $\frac{d\Delta_{\perp}}{dr}$ is an additional input parameter available in BETACOOOL simulations.

An example of simulations of the cooling (using BETACOOOL) is presented in the Fig. I.A.2.2. The red curve correspond to an average momentum of the antiprotons. The first 1700 sec correspond to pre-cooling of the antiprotons. At $t=1700$ sec, the electron momentum was shifted by the relative value of 10^{-3} and during the next 2000 sec the average antiproton momentum is cooled to the new momentum of the electrons. The green curve presents the variation in time of the antiproton momentum spread.

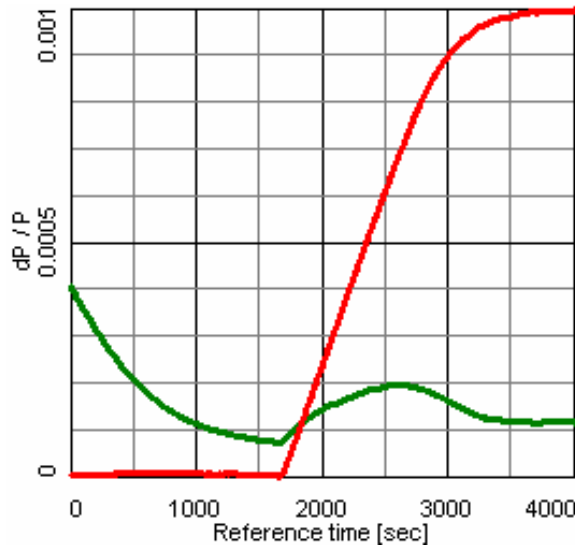


Fig. I.A.2.2. Simulation of the voltage step method using BETACOOOL program, for the parameters shown in Table I.A.2.1.

Table I.A.2.1. The Recycler cooling system parameters used in simulations.

Cooling section length, m	20
Electron energy, MeV	4.36
Beta functions in the cooling section, m	20
Electron current, A	0.2
Electron beam radius, cm	0.45
Transverse temperature (PRF), eV	0.5
Longitudinal temperature (PRF), eV	0.01

Evolution of the antiproton momentum during the friction force measurement, as a 3D plot of the profile versus time, is shown in Fig I.A.2.3.

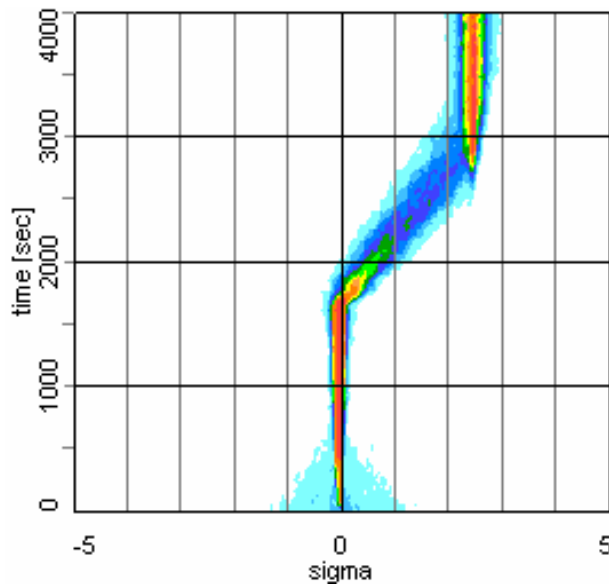


Fig. I.A.2.3. The longitudinal profile evolution during friction force measurement.

To reproduce the procedure used in Fermilab for the beam longitudinal distribution measurement the possibility to average over a few consequent longitudinal profiles was also introduced. An example of a few consequent averaged profiles calculated with BETACOOOL after 2 keV step of the electron energy is presented in the Fig. I.A.2.4. The electron beam current is 500 mA. Figure I.A.2.5 shows measured profiles for the same parameters.

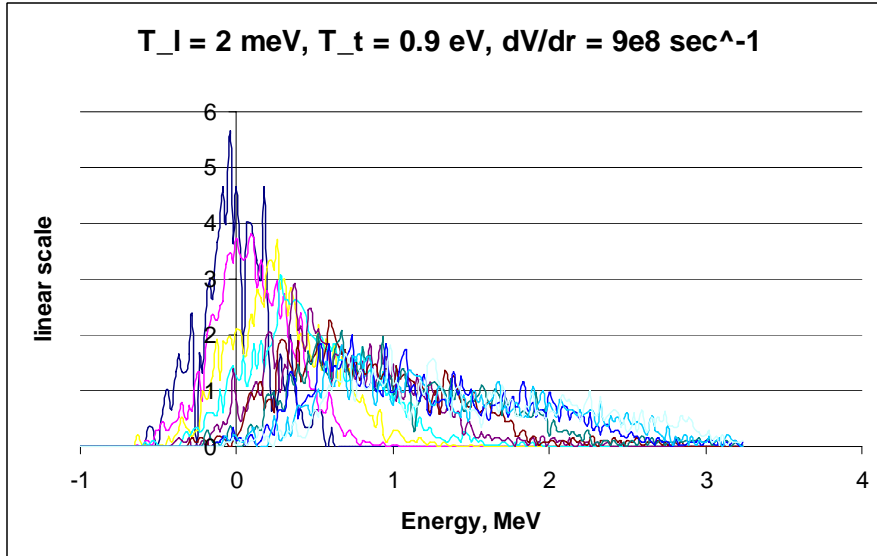


Fig. I.A.2.4. Simulations (A. Sidorin, JINR). Evolution of the longitudinal profile in time. Distance between slices is 50 sec.

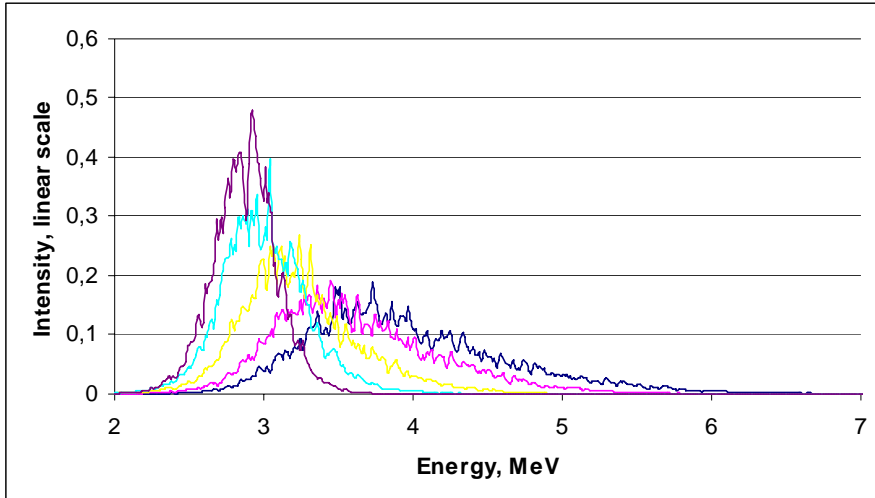


Fig. I.A.2.5. Measurements (L. Prost, FNAL). Evolution of the longitudinal profile in time.

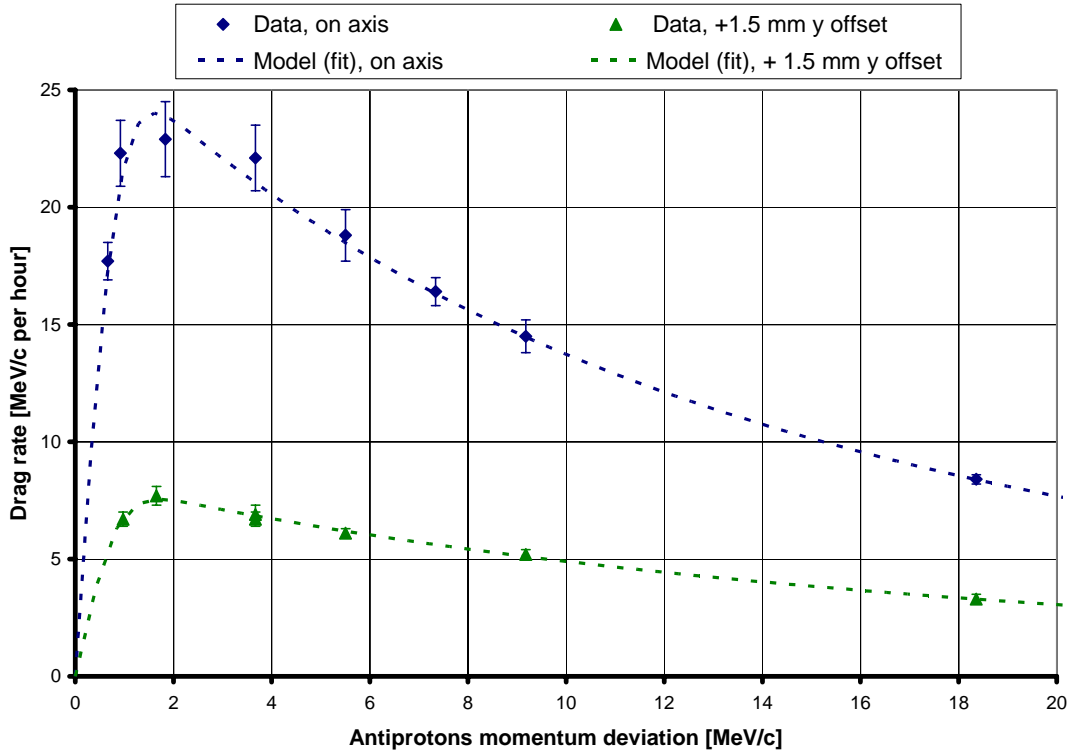


Fig. I.A.2.6. (Courtesy of L. Prost, A. Shemyakin, FNAL). Measurements vs theoretical model.

Analysis of the experimental data and comparison with theory is being done in collaboration with the electron cooling groups of Fermilab (S. Nagaitsev, L. Prost, A. Shemyakin, A. Burov) and JINR (A. Sidorin and A. Smirnov).

Presently, the agreement between the theory and experiments is about factor of 2 [16]. Such an uncertainty is attributed to the uncertainties/assumptions about the electron beam characteristics. More details on the results of benchmarking can be obtained from the Fermilab group.

I.A.2.4. Friction force in the presence of an undulator field

Suppression of the ion recombination for RHIC is based on the use of an undulator field in the cooling section [8, 9]. In the presence of an undulator field, the trajectories of all the electrons have the same coherent azimuthal angle θ , determined by the undulator period λ and field value B at the axis:

$$\theta = \frac{eB\lambda}{2\pi pc}, \tag{I.A.2.17}$$

where p is the electron momentum. Since the recombination cross section is approximately inversely proportional to the electron energy in the ion rest frame, the ion beam life time can be sufficiently improved.

One can expect that at impact parameters significantly larger than the electron rotation radius

$$r_0 = \frac{\theta\lambda}{2\pi} = \frac{eB\lambda^2}{4\pi^2 pc} \quad (\text{I.A.2.18})$$

kinematics of the binary collisions will be similar to Rutherford scattering of free electron. In this case the friction force acting on the ion inside the electron beam with the velocity distribution function $f(v_e)$ can be still calculated with the usual formula:

$$\vec{F} = -\frac{4\pi m_e e^4 Z^2}{m} \int L_c \frac{\vec{V}_i - \vec{v}_e}{|\vec{V}_i - \vec{v}_e|^3} f(v_e) d^3 v_e, \quad (\text{I.A.2.19})$$

where n_e is electron density in the Particle Rest Frame (PRF), v_e , V_i are the electron and ion velocity, L_c – Coulomb logarithm:

$$L_c = \ln \frac{\rho_{\max}}{\rho_{\min}}. \quad (\text{I.A.2.20})$$

For the RHIC parameters, the maximum impact parameter is determined by the time of flight of the ion through the cooling section and it is not affected by the undulator field. However, the minimum impact parameter ρ_{\min} which is determined by a relative velocity between an ion and electron as

$$\rho_{\min} = \frac{Ze^2}{m_e} \frac{1}{|\vec{V}_i - \vec{v}_e|^2}, \quad (\text{I.A.2.21})$$

has to be replaced by r_0 value, in the presence of the undulator field. Therefore, the friction force is expected to be reduced by the factor of the order of $\ln \frac{\rho_{\max}}{\rho_{\min}} / \ln \frac{\rho_{\max}}{r_0}$.

To make sure that such a representation of the friction force in the presence of an undulator field is accurate, an undulator field was implemented in the VORPAL code, and numerical simulations were performed (G. Bell et al.) [17] for different strength of the magnetic field B and pitch period λ .

An example of such a comparison between VORPAL simulations (dots with error bars) and numeric integration with the BETACOOOL (lines) is shown in Figs. I.A.2.7-8, for an rms ion velocity of $3.0 \cdot 10^5$ [m/s] in PRF and the following parameters in simulations ($\Delta_{\perp} = 3.0 \cdot 10^5$ [m/s] and $\Delta_{\parallel} = 3.0 \cdot 10^5$ [m/s], $\tau = 0.9$ nsec, $Z = 79$, $n_e = 7.32 \cdot 10^{13}$ m⁻³).

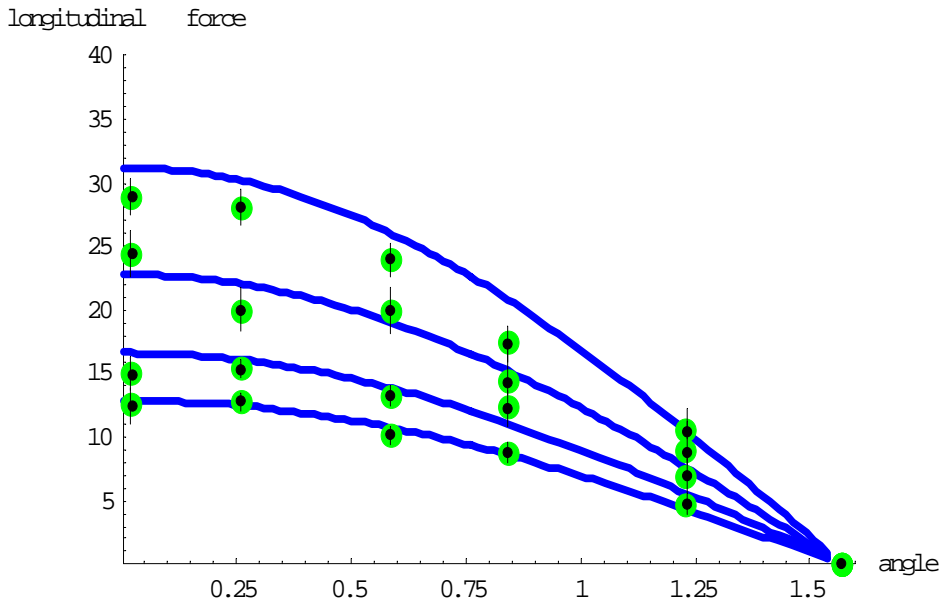


Fig. I.A.2.7. Longitudinal component of the friction force at an rms ion velocity of $3.0 \cdot 10^5$ m/s for B=0 (upper curve) and for an undulator with different periods $\lambda=8, 16, 24$ cm (B=10G). VORPAL – dots with error bars; BETACOOOL numerical integration – lines.

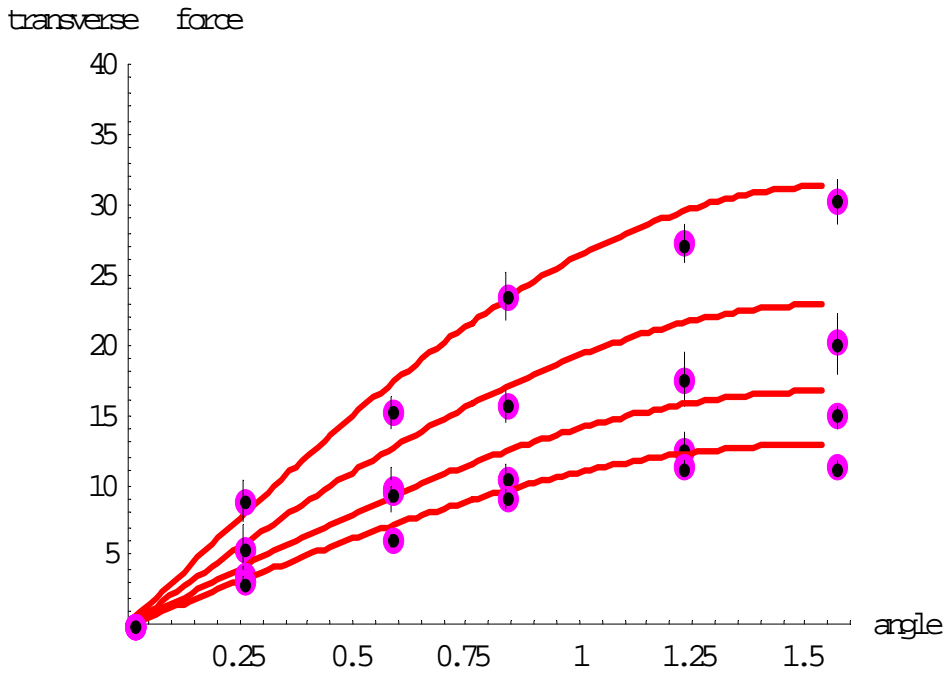


Fig. I.A.2.8. Transverse component of the friction force at an rms ion velocity of $3.0 \cdot 10^5$ m/s for B=0 (upper curve) and for an undulator with different periods $\lambda=8, 16, 24$ cm (B=10G). VORPAL – dots with error bars; BETACOOOL numerical integration – lines.

In all cases, it was found that the friction force scales as predicted by a modified logarithm $\ln \frac{\rho_{\max}}{r_0}$.

Impact of undulator fields was further investigated by including errors in the alignment of individual sections of the undulator. Even with relatively high offsets of 3mm no significant effect on the friction was observed. The study of the effects of errors on the friction force is continuing.

Figure I.A.2.9 shows that the force with the random offset between individual undulator sections of 3 mm is the same as the force without misalignments. Simulations in the figure are done for the present baseline parameters of the electron beam and undulator, and observed reduction in the force values in the presence of undulator field is as expected. With such a reduction in the force values, the recombination rates can be suppressed by an order of magnitude.

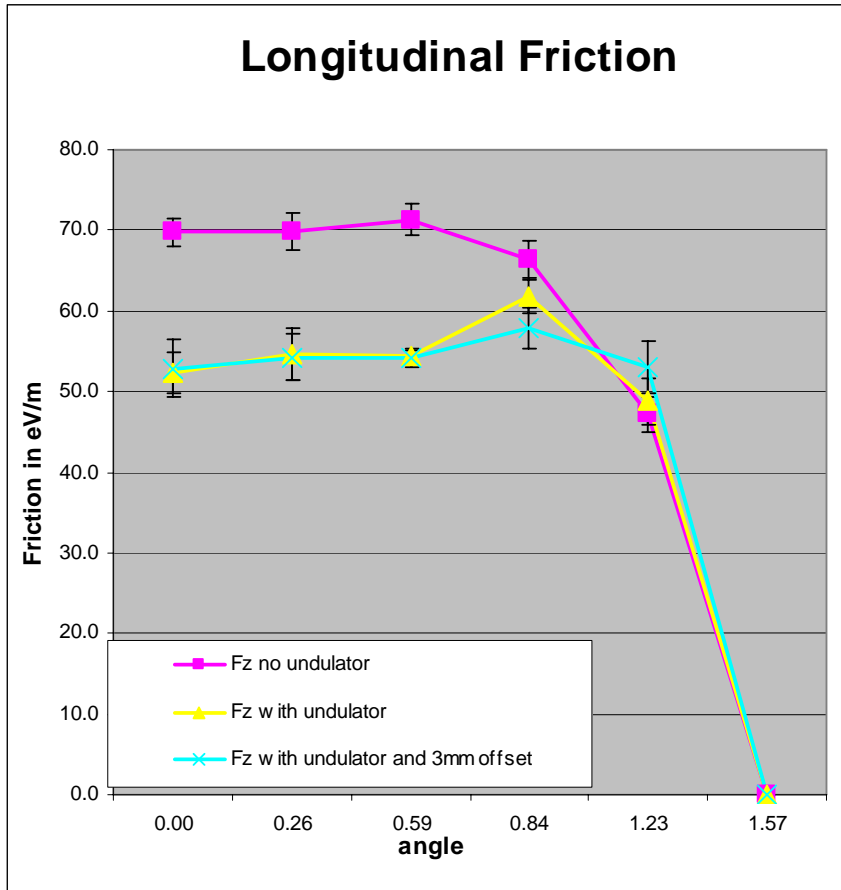


Fig. I.A.2.9. (Courtesy of G. Bell, Tech-X Corp.) VORPAL simulations: Longitudinal component of the friction force [eV/m] vs angle [rad] of velocity vector with respect to the longitudinal axis. The plot is done for the amplitude of ion velocity vector of $3.0 \cdot 10^5$ m/s for an undulator with period $\lambda=8$ cm ($B=10G$).

I.A.3. Intrabeam scattering

Charged particle beams are stored in circular accelerators for a long time. The phenomenon when particles within the beam are scattered from one another via Coulomb scattering is called Intra-Beam Scattering (IBS). Such a process is typically separated in two effects:

1. Scattering on a large angle so that the particles can be lost from a bunch as a result of a single collision – such an effect is called the Touschek effect.
2. Scattering on small angles can randomly add together which can cause beam dimension to grow – such effect is called the Intra-Beam Scattering.

I.A.3.1 General models

The process of IBS is very similar to collisions in a plasma (ionized gas), which govern gas relaxation towards equilibrium. The corresponding simple diffusion coefficients can be derived. The case of charged particle beam is in fact very similar to the plasma case when the longitudinal motion is transformed away by going into the Particle-Rest-Frame (PRF) which moves along the storage ring at the nominal beam velocity. The scattering events now appear exactly as in the plasma case, the only difference is that the distribution function is now given in terms of generalized coordinates which describe particle motions in circular accelerator. In circular accelerator, curvature of the orbit produces a dispersion, and due to the dispersion a sudden change in energy results in a change of betatron amplitudes. Such a coupling makes an important difference between small-angle Coulomb collisions in plasma (Gas-Relaxation) and in circular accelerators (IBS).

A theory of IBS for proton beams was proposed by Piwinski [18], who calculated the beam growth rates in all three dimensions. In the original theory, growth rates were estimated as an average around the circumference of the ring. For this purpose, the ring lattice functions were also averaged. This model was later extended by a CERN team in collaboration with Piwinski to include variations of the lattice function around the ring. An improved model was later described in a detailed report by Martini [19] and is sometimes referred to as Martini's model. Similar results were also obtained with a completely different approach of S-matrix formalism by Bjorken and Mtingwa [20].

For RHIC parameters, results using both Martini's and Bjorken-Mtingwa's models were found to be in a very good agreement with one another. For our numerical studies of electron cooling presented in this report the Martini's model was used without any approximation. We also used an exact designed lattice of RHIC which includes the derivatives of the lattice functions and insertions in the straight sections for the IP's.

The standard IBS theories were developed in the assumption of uncoupled betatron motion. A more general treatment for the coupled motion was also developed by Piwinski [18] and recently by Lebedev [21]. The standard RHIC operation corresponds to the working point in the vicinity of the coupling resonance with the fully coupled motion. In such a case, the standard treatment of IBS can be used with the horizontal growth rate equally shared between the horizontal and vertical motion – such an assumption was found to be in good agreement with experimental measurements and is presently used in simulations.

I.A.3.2 IBS in RHIC: experiments vs theory

Since the main goal of electron cooling is to overcome emittance growth due to IBS, it was extremely important to make sure that the models of IBS which are being used in cooling simulations are in a good agreement with experimentally measured growth rates.

Several dedicated IBS experiments were performed in 2004 with Au and in 2005 with Cu ions with an intention to increase accuracy and parameter range of previous measurements [22]. To ensure an accurate benchmarking of the IBS models, bunches of various intensity and emittance were injected, and growth rates of both the horizontal and vertical emittance and the bunch length were recorded with IPM and WCM, respectively. Other effects which may obscure comparison, like beam-beam collisions, were switched off. Experiments were done with the RF harmonic $h=360$ allowing growth of the longitudinal profile without any loss from the bucket.

Although, agreement for the longitudinal growth rate was very good for the 2004 measurements with the Au ions, agreement for the transverse emittance was not that perfect [23]. In fact, the measured transverse emittance growth was larger than the one predicted by simulation using Martini's model of IBS with the exact designed RHIC lattice. As a result of the 2004 studies, a fudge factor was introduced for the transverse growth rate of IBS to make sure that we do not underestimate IBS growth rate for the cooling simulations. Subsequent cooling simulations were done to compensate for such an "enhanced" IBS.

Following the 2004 measurements several studies were done trying to understand a possible source of the disagreement, including IBS growth for the lattice with different average dispersion functions, FODO approximation for the lattice vs. realistic RHIC lattice with straight-section insertions, dispersion mismatch and others [24]. As a result of these studies, it was decided to repeat the measurements with the Cu ions in 2005.

The latest data for IBS with Cu ions showed very good agreement between the measurements and Martini's model of IBS for designed RHIC lattice without any approximation or previously used fudge factors [25]. Below, few examples from these studies are shown in Figs. I.A.3.1-3.

Figure I.A.3.1 shows growth of the horizontal and vertical emittance in bucket # 100 with the bunch intensity $2.9 \cdot 10^9$.

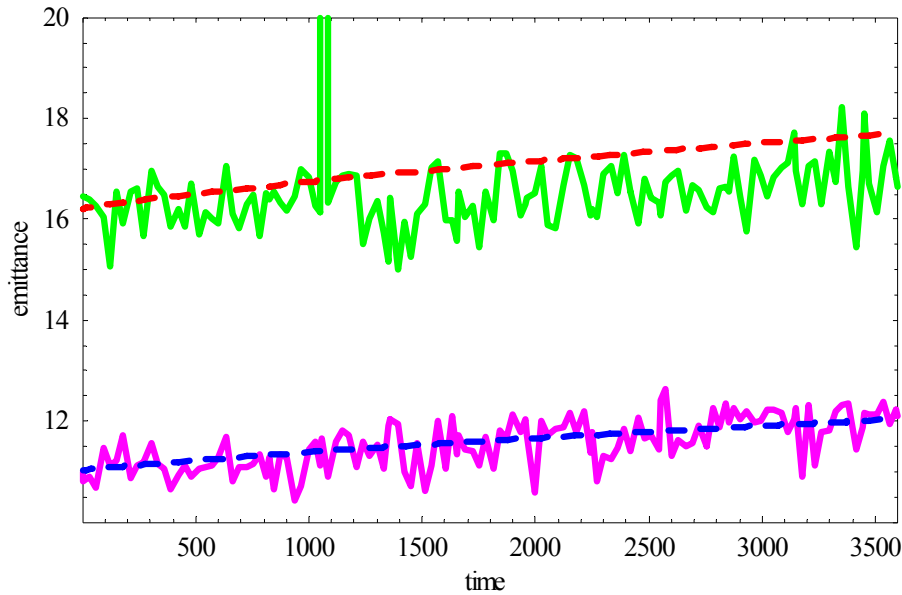


Fig. I.A.3.1 Horizontal (upper curve) and vertical 95% normalized emittance [mm mrad] vs time [sec] for bunch intensity $2.9 \cdot 10^9$ Cu ions. Measured emittance: green (horizontal), pink (vertical). BETACOO simulation using Martini's model: red dash line (horizontal), blue dash line (vertical).

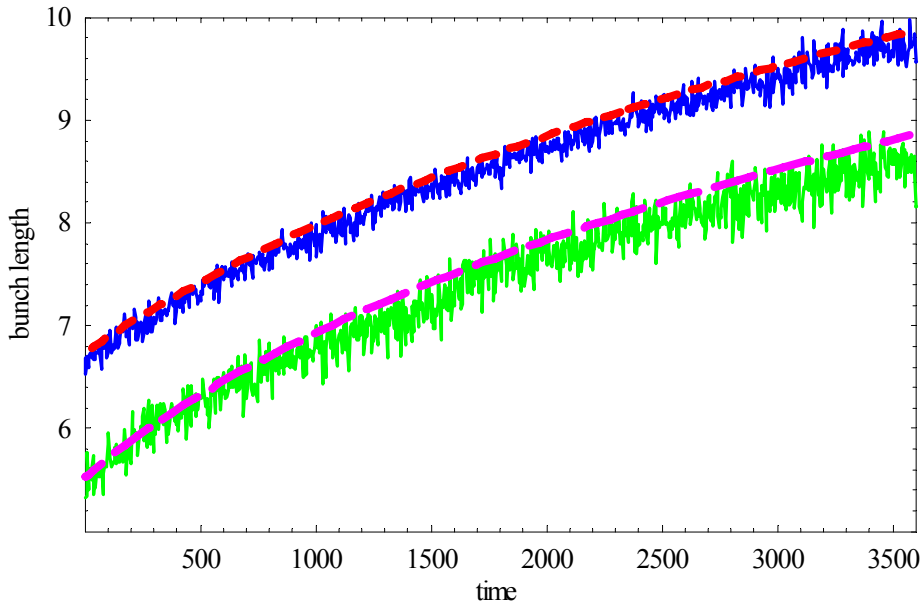


Fig. I.A.3.2 Growth of FWHM bunch length [ns] vs time [sec] for two bunch intensities: $2.9 \cdot 10^9$ (upper curve) and $1.4 \cdot 10^9$ (lower curve) Cu ions.

Measured growth rates scale correctly with the bunch intensity and the value of the initial emittance, as shown for the two intensities in Fig. I.A.3.2 and Fig. I.A.3.3 for the bunch length and horizontal emittance, respectively.

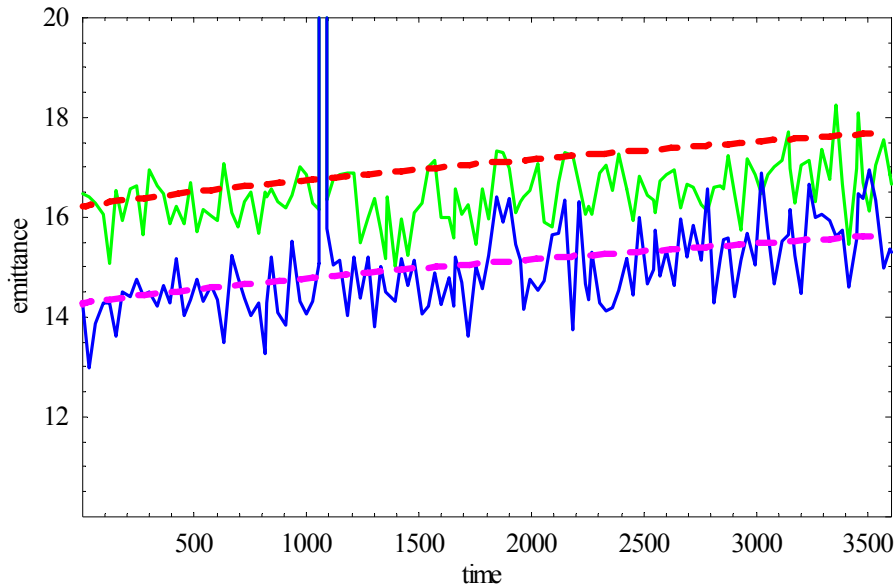


Fig. I.A.3.3 Horizontal 95% normalized emittance [μm] for two bunch intensities: $2.9 \cdot 10^9$ (upper curve) and $1.4 \cdot 10^9$ (lower curve) Cu ions.

More details about comparison of IBS measurements in RHIC with the models can be found in [25].

I.A.3.3 IBS for ion beam distribution under electron cooling

Standard models of IBS discussed above are based on the growth rates of the rms beam parameters for the Gaussian distribution. However, as a result of electron cooling, the core of beam distribution is cooled much faster than the tails. For previous parameters of the magnetized cooling it was found that a simple use of standard rms-based IBS approach would significantly underestimate IBS for beam core. A detailed analytic treatment of IBS, which depends on individual particle amplitude was proposed by Burov [26], with an analytic formulation done for a “flattened” Gaussian distribution. Also, a simplified “core-tail” model, based on a different diffusion coefficients for beam core and tails was also proposed [27]. In addition, the standard IBS theory was reformulated for the rms growth rates of a bi-Gaussian distribution by Parzen [28].

The above formulations, which attempt to calculate IBS for a beam distribution changing under electron cooling, were implemented in BETACOOOL [1] and were used for cooling studies of RHIC [27]. The difference between various models and resulting integrated luminosity was found to be substantial for the previous approach of the magnetized cooling where a formation of a distribution with a sharp core was observed.

For the present parameters of the non-magnetized cooling, the formation of such a bi-Gaussian distribution is less pronounced than before for the case of the magnetized cooling. As a result, a deviation between various models and the difference in the integrated luminosity being predicted is expected to be less crucial, although it is probably the largest source of uncertainty in present simulations with the “Modeled Beam” approach. More detailed algorithms for the IBS are presently being developed to reduce remaining uncertainty.

I.A.4 Recombination

I.A.4.1 Numerical algorithm

Ion beam life time due to recombination

The ion beam life time due to recombination in the cooling section is calculated via recombination coefficient α_r by the following formula:

$$\frac{1}{N} \frac{dN}{dt} = -\frac{\alpha_r n_e l_{cool}}{\gamma^2 C}, \quad (\text{I.A.4.1})$$

here C is the ring circumference. Under assumption that ion velocity in PRF is substantially less than the one of the electrons, recombination coefficient α_r is calculated in PRF by averaging of the recombination cross section over electron distribution function:

$$\alpha_r = \langle v \sigma(v) \rangle \quad (\text{I.A.4.2.})$$

The recombination cross section can be calculated with good accuracy using the following formula:

$$\sigma = A \left(\frac{h\nu_0}{E} \right) \left(\ln \sqrt{\frac{h\nu_0}{E}} + 0.1402 + 0.525 \left(\frac{E}{h\nu_0} \right)^{1/3} \right), \quad (\text{I.A.4.3})$$

where $A = 2^4 3^{-3/2} h e^2 / (m_e^3 c^2) = 2.11 \times 10^{-22} \text{ cm}^2$, $h\nu_0 = 13.6 \cdot Z^2 \text{ eV}$ is the ion ground state binding energy, and $E = \frac{m_e v_e^2}{2}$ is the kinetic energy of the electrons. In the presence of the undulator field the kinetic energy needs to be calculated as:

$$E = \frac{m}{2} \left((v_{\perp} + v_{und})^2 + v_{\parallel}^2 \right), \quad (\text{I.A.4.4})$$

The formula (I.A.4.2) can be rewritten in the form adopted for numerical integration:

$$\alpha_r = \frac{1}{Int} \int_0^{3\Delta_{\perp}} \int_{-3\Delta_{\parallel}}^{3\Delta_{\parallel}} \sigma(E) \sqrt{(v_{\perp} + v_{und})^2 + v_{\parallel}^2} \exp \left(-\frac{(v_{\perp} + v_{und})^2}{2\Delta_{\perp}^2} - \frac{v_{\parallel}^2}{2\Delta_{\parallel}^2} \right) v_{\perp} dv_{\parallel} dv_{\perp}. \quad (\text{I.A.4.5})$$

The normalization factor is calculated as:

$$Int = \int_0^{3\Delta_{\perp}} \int_{-3\Delta_{\parallel}}^{3\Delta_{\parallel}} \exp \left(-\frac{(v_{\perp} + v_{und})^2}{2\Delta_{\perp}^2} - \frac{v_{\parallel}^2}{2\Delta_{\parallel}^2} \right) v_{\perp} dv_{\parallel} dv_{\perp}. \quad (\text{I.A.4.6})$$

Here

$$\Delta_e = \sqrt{\Delta_{\perp}^2 + \Delta_{\parallel}^2} \quad (\text{I.A.4.7})$$

is an rms electron velocity spread, with the electron beam temperature being different for the transverse and longitudinal degrees of freedom. The expression in Eq. (I.A.4.5) is being used in BETACOOOL to calculate recombination rate for RHIC.

I.A.4.2 Experimental measurements and theory.

Radiative recombination of ions was extensively studied experimentally. Perfect agreement between measurements and theoretical prediction for the recombination coefficient was found in a wide range of relative energies between the electrons and ions ($>10\text{meV}$). However, in the region of extremely small relative energies (which is the region typically used for electron cooling), the measured recombination coefficient for experiments with bare ion was found significantly higher than predicted by standard theory of radiative recombination (for ions which are not fully stripped there is an additional channel via dielectronic recombination which is not discussed here).

The surprising discrepancy between widely recognized theory and measurements resulted in variety of theoretical studies which attempted to address this issue. They range from the influence of three body recombination and density enhancement due to plasma screening effects to the effects of magnetic field on the cross section. However, none of the proposed models was able to account quantitatively for the measured enhancement of recombination coefficients until recently [29].

In the newly proposed model [29], the merging of electron and ion beam results in bound states which in combination with the radiative stabilization due to a strong magnetic field in a cooling solenoid (typical set-up in low-energy coolers) yield a substantial population of low-lying states in the recombined system. The magnitude of the resulting recombination rates in simulations agreed with measurements very well. Scaling on ion charge Z and strength of the magnetic field B also agreed with measurements.

In this latest theoretical model [29], which explains the enhancement in the recombination observed, the presence of strong magnetic field in the cooling section is important in radiative stabilization process. This mechanism is not expected to occur in the absence of the solenoidal magnetic field. In addition, in the case of RHIC cooling, the presence of undulator field increases the relative energy to about 30 eV. The agreement between theoretical and experimental recombination coefficient at such high relative energies is very good [30].

I.A.4.3 Parameters of the undulator

Table I.A.4.1 Parameters of the undulator

Magnetic field [G]	10
Period [cm]	8
Introduced effective temperature T_{eff} [eV]	30
Recombination lifetime with T_{eff} [hours]	166

I.A.5 Detailed calculation of the cooling dynamics

I.A.5.1 Baseline parameters

Table I.A.5.1 Present parameters

Electron kinetic energy [MeV]	54.34
Number of electrons per bunch	$3 \cdot 10^{10}$
Electron charge per bunch [nC]	5
Ion beta functions in the cooling section [m]	400
Ion rms beam radius [mm]	3
Ion initial rms bunch length [cm]	20
Circumference of RHIC ring [m]	3833
Electron cooler length [m]	80
Rms electron beam emittance normalized [$\pi \cdot \text{mm} \cdot \text{mrad}$]	4
Electron rms momentum spread	$3 \cdot 10^{-4}$
Ion initial rms momentum spread	$5 \cdot 10^{-4}$
Transverse rms radius of electron beam [mm]	4.3
Electron rms bunch length [cm]	1
Relativistic factor γ (ions, electrons)	107.35
Transverse rms angles of ions in cooling section [μrad]	7.6
Transverse rms angles of electrons [μrad]	8.7

I.A.5.2 Detailed evolution of beam distribution

A quick estimate of the cooler performance can be done using an approach with a dynamical tracking of the rms beam parameters. This approach was found to be too inaccurate for previous design with the magnetized cooling for RHIC when a detailed treatment of the beam distribution was found to be extremely important. For the case of a fast cooling in typical low-energy coolers where the whole Gaussian beam is quickly cooled to an approximately Gaussian beam with much smaller rms parameters, a simple approach based on an rms dynamics provides reasonably accurate estimates. For the present parameters of the RHIC cooler based on the non-magnetized approach most of the particles within few sigmas are also effectively cooled, making an rms dynamics approach a reasonable estimate as well. The luminosity prediction based on such an rms approach is shown in Fig. I.A.5.1.

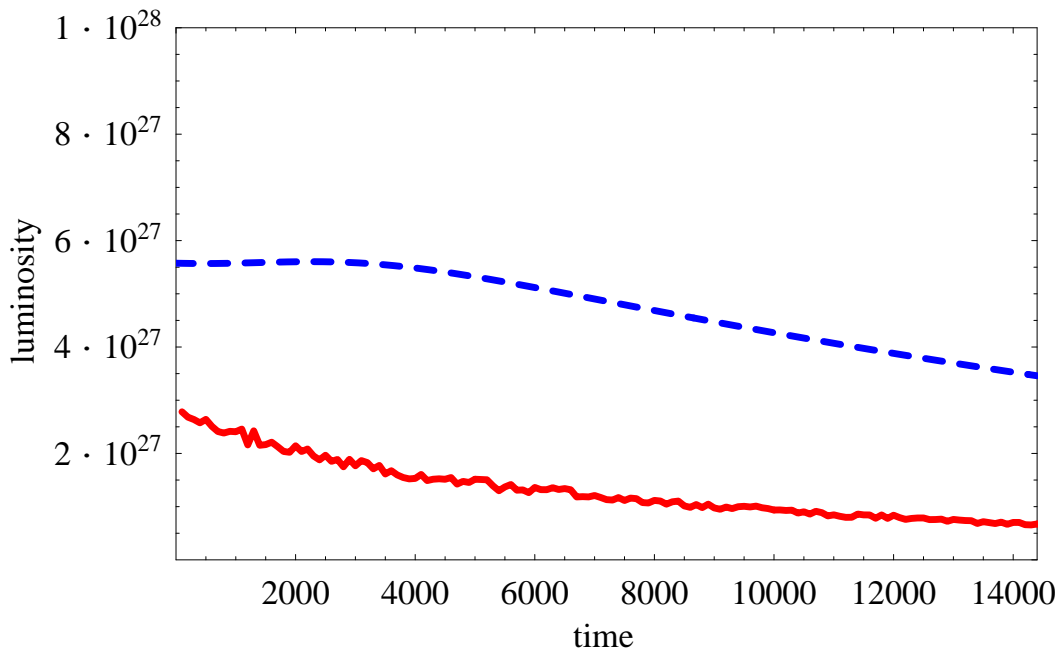


Fig. I.A.5.1 Luminosity of Au ions [$\text{cm}^2 \text{s}^{-1}$] vs time [sec] for RHIC-II without cooling (red) and with cooling (blue) based on simulations with the “rms dynamics” approach, for cooler parameters in Table I.A.5.1.

The average luminosity with cooling in Fig. 1.A.5.1 is only $\langle L \rangle = 5 \cdot 10^{27} \text{ [cm}^2 \text{sec}^{-1}]$, which can be further increased by using higher charge of the electron beam and smaller beta-function at the IP. Note, that such an estimate is based on the rms dynamics (which is a very simplified model) and, in some sense, is a low-limit estimate for the luminosity increase.

A more accurate treatment is to use a numerical approach which allows one to track evolution of the beam distribution. Such an approach requires accurate calculation of many effects from a real distribution, including loss on recombination, burn-off process, IBS and calculation of the luminosity from the local charge density. All these algorithms are implemented in BETACOOOL and are being used under the “Modeled beam” approach (which is sometimes is referred to as “detailed” approach since its based on details of the distribution).

However, each of these effects contributes to the uncertainty (numerical effects and accuracy of the models being used) in the simulations. The effect which results in the largest uncertainty (due to an approximate model) is the treatment of IBS for non-Gaussian distribution. Presently, depending on the model being used, the final result can be different by as much as 20-30%. To remove this largest source of uncertainty new numerical algorithms are being developed within the BETACOOOL to describe IBS for an arbitrary distribution more accurately.

Figures I.A.5.2-4 show evolution of the horizontal (red), vertical (blue) and longitudinal (green) beam profiles after 0.5, 1.5 and 2.5 hours of cooling, respectively. Simulations were done for the parameters in Table I.A.5.1 using the “Modeled beam” approach in BETACOOOL. The corresponding luminosity with and without cooling is shown in Fig. I.A.5.5.

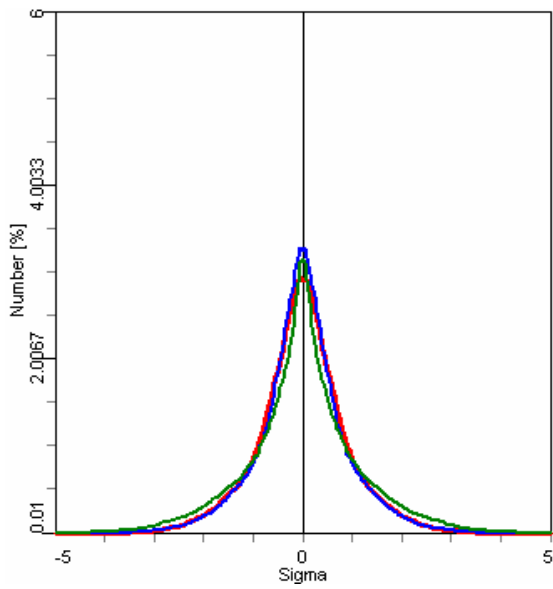


Fig. I.A.5.2 Beam profiles (x-red, y-blue, longitudinal -green) after 30 minutes of cooling

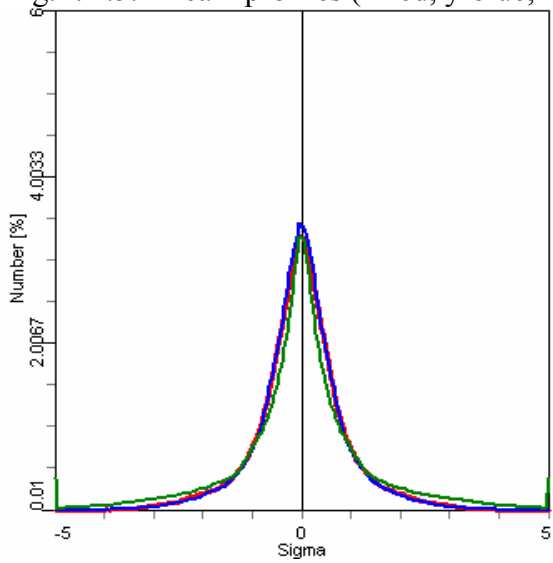


Fig. I.A.5.3 Beam profiles after 1.5 hours of cooling.

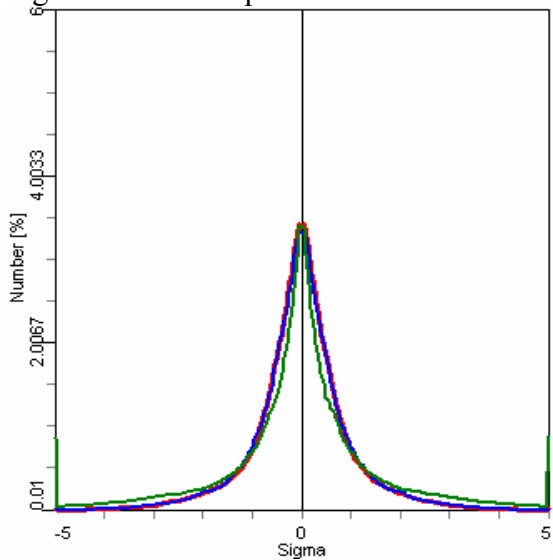


Fig. I.A.5.4 Beam profiles after 2.5 hours of cooling.

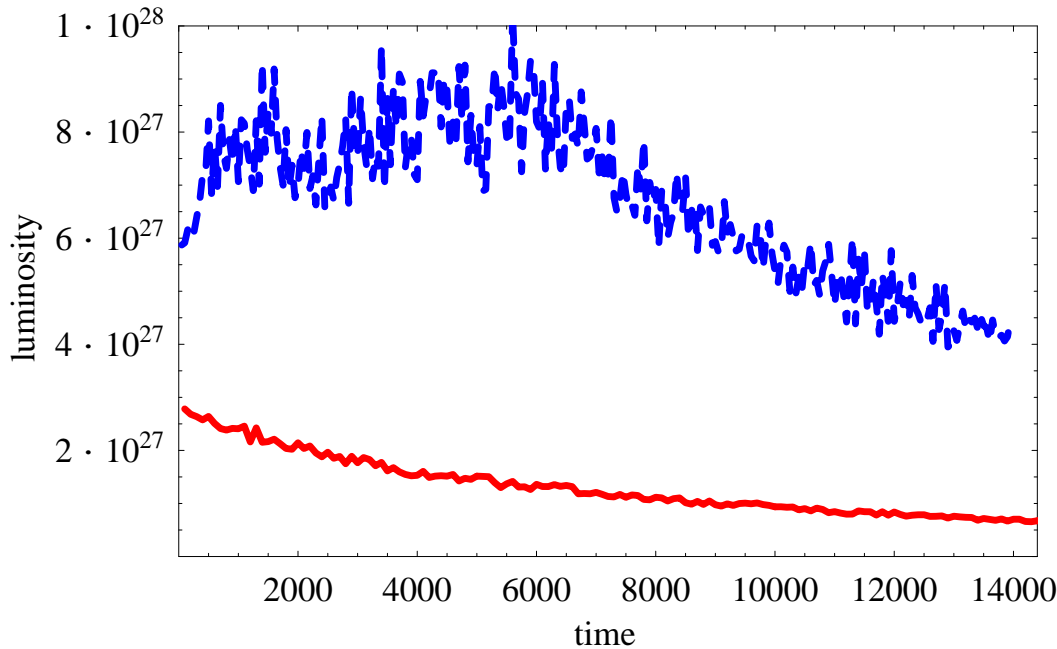


Fig. I.A.5.5 Luminosity of Au ions [$\text{cm}^2 \text{s}^{-1}$] vs time [sec] with (blue) and without (red) cooling using “Modeled beam” approach in BETACOOOL simulations for parameters in Table I.A.5.1.

Although predicted integrated luminosity in Fig. I.A.5.5 appears to be higher than the one predicted based on the rms approach, the uncertainty in its value is larger as well. For the case shown in Fig. I.A.5.5, average luminosity with cooling (blue) per store is $\langle L \rangle = 7 \cdot 10^{27} [\text{cm}^2 \text{sec}^{-1}]$. Without cooling, Fig. I.A.5.5 shows “ideal” luminosity which may be possible to achieve which corresponds to about $\langle L \rangle = 1 \cdot 10^{27} [\text{cm}^2 \text{sec}^{-1}]$. More pragmatic estimate for luminosity of RHIC-II without cooling gives $\langle L \rangle = 0.8 \cdot 10^{27} [\text{cm}^2 \text{sec}^{-1}]$.

Some additional luminosity increase may come from the painting with the electron beam (which we need to do since the length of the electron bunch is much smaller than the one of the ions), which is discussed in Section I.A.6. Also, further increase in luminosity is possible by going to higher charge of the electron beam and smaller beta function in the IP but the optimum time of store becomes rather short.

I.A.5.3 Requirements on transverse emittance of electron beam

Ideally, one would like to have the transverse rms velocity spread of the electron beam to be comparable or smaller than the one of the ions. Since the normalized rms emittance of ions is $2.5 \mu\text{m}$ an ideal electron emittance should be slightly below $2.5 \mu\text{m}$. However, the necessary cooling power requires charge within electron bunch to be around 5nC . A preliminary simulations with electron beam showed that the electron emittance of $4 \mu\text{m}$ can be achieved. The sizes of the ion and electron beam in the cooling section were optimized so that the rms normalized emittance of $4 \mu\text{m}$ provides sufficient cooling power.

Recent progress in simulations of electron beam transport indicates that for 5nC charge of electron beam one can obtain transverse emittance better than $4 \mu\text{m}$. However, there are many other effects

which can impact electron beam quality. Such effects are presently under study. For simulations presented in this report the value for emittance of $4 \mu\text{m}$ was used.

In terms of rms angles, with the ions beta function of 400 m in the cooling section, the rms angular spread of ion beam is only $\theta_i=7.6 \mu\text{rad}$. This puts an extremely challenging requirement to control angles in the electron beam (with contributions coming from various effects) to just $10 \mu\text{rad}$ or better. Cooling simulations described in this report are done for the electron angles in the cooling section of $\theta_e=8.7 \mu\text{rad}$.

I.A.5.4 Requirements on longitudinal momentum spread of electron beam

The rms momentum spread of the ion beam is about $0.5 \cdot 10^{-3}$. An effective longitudinal cooling is obtained with the rms momentum spread of the electron beam around $0.3 \cdot 10^{-3}$. Simulations were performed to find out requirement on the average electron beam energy. The cooling efficiency was significantly affected when the average energy of the electron beam became comparable or bigger than the rms energy spread of the ion beam. This sets a requirement on average energy deviation of the electron beam to be around $0.3-0.5 \cdot 10^{-3}$.

I.A.5.5 Cooling with realistic 6-D distribution of electrons

Typical evaluation of the friction force is done based on the rms parameters of the electron bunch as a whole (projected rms emittances and momentum spread), as described by Eqs. (I.A.2.12)-(I.A.2.14). However, both the rms emittance and energy spread can be different in different longitudinal slices along the electron bunch. To take this into account, the algorithm of “Local Electron Beam” distribution was implemented in BETACOOOL which allows to calculate and use local rms parameters within the bunch for the friction force evaluation based on the realistic 6-D distribution of the electrons obtained with the PARMELA code. As an extension of this algorithm, the friction force can be calculated for an arbitrary distribution of the electrons without assumption that velocity distribution of electrons is Maxwellian. These new algorithms are presently being studied for numerical convergence and will be compared vs standard approach with the rms parameters. The goal of these studies is to produce accurate requirements on the quality of the electron beam needed for cooling.

I.A.5.6 Cooling optimization

Major parameters which affect beam cooling are:

1. Length of cooling section – directly impacts cooling speed.
2. Cooling current – directly impacts cooling speed.
3. Dependence on beta-function in the cooling solenoid – partially offset by ion beam size increase – corresponding increase of electron beam size leads to reduction of electron density.
4. Alignment of electron-ion beam.
5. Transverse and longitudinal rms velocity spread within electron beam.

For the charge of the electron beam other than 5nC as well as β^* other than 50cm the length of the store is also optimized

I.A.5.7 Cooling performance with and without recombination suppression

The undesired beam loss due to recombination can be controlled by an undulator field in the cooling section. However, the resulting friction force with the undulator field is reduced, which was confirmed by the simulations (see Section I.A.2.4). As a result, depending on the parameters of the electron beam and the cooler, there may be even a small loss in the integrated luminosity with the undulator field being switched on compared to the case with the undulator switched off. For the present baseline parameters in Table I.A.5.1, the integrated average luminosity is higher with the undulator switched on. This is shown in Figs. I.A.5.6-8.

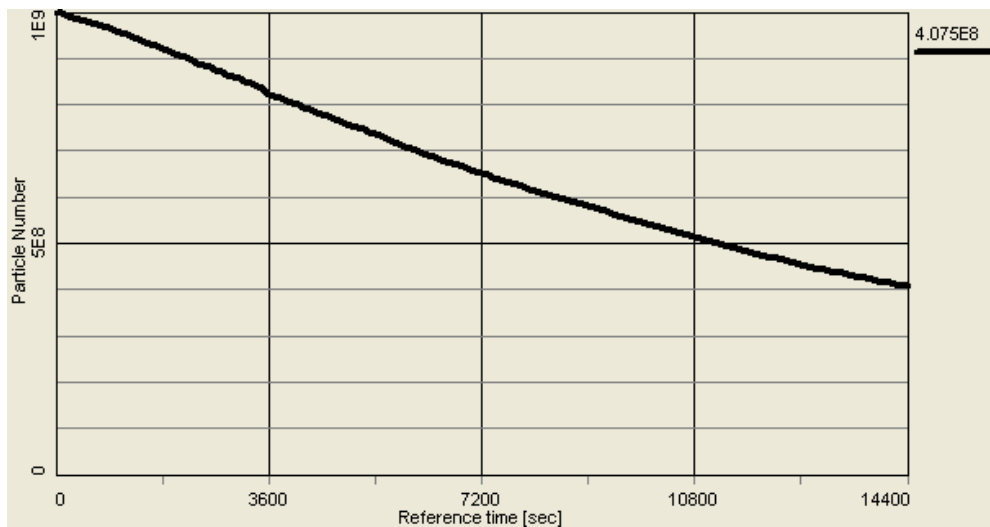


Fig. I.A.5.6 Particle loss only due to collisions in 3 IP (recombination loss is turned off).

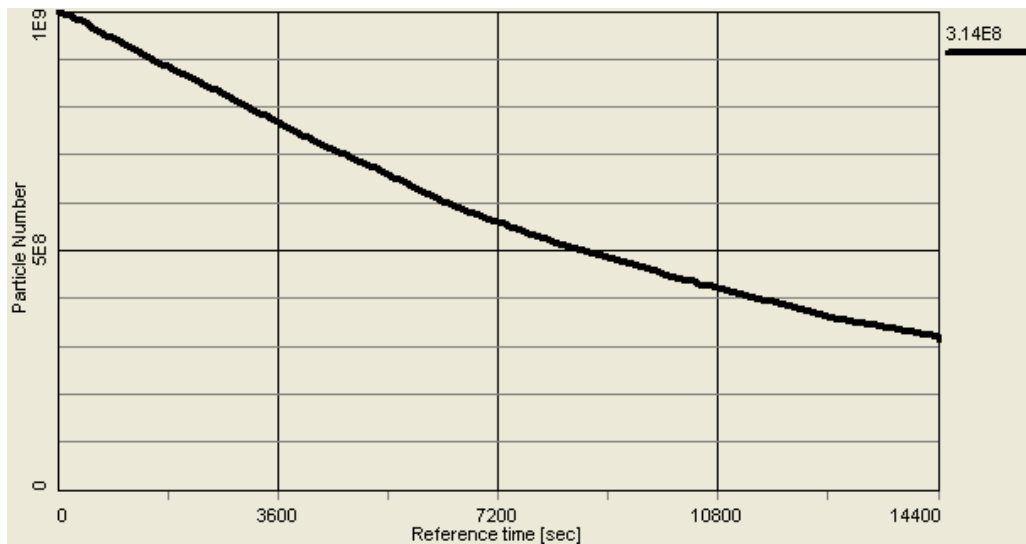


Fig. I.A.5.7 Particle loss due to collisions in 3 IP and recombination in the cooler.

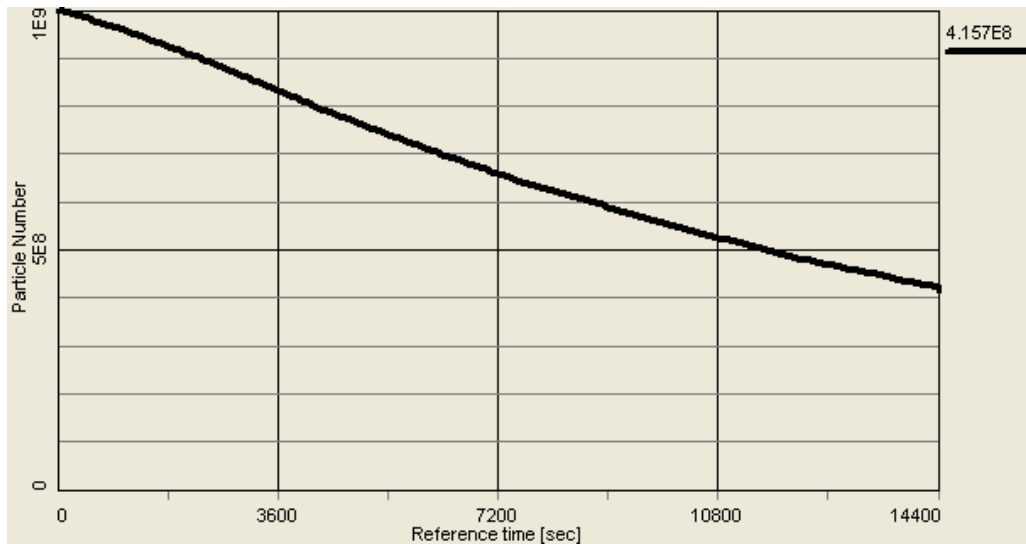


Fig. I.A.5.8 Particle loss due to collisions in 3 IP, recombination in the cooler, and undulator with parameters in Table I.A.4.1.

For parameters in Table I.A.5.1, as a result of loss on recombination, an average luminosity during 4-hour store is $\langle L \rangle = 6 \cdot 10^{27} [\text{cm}^2 \text{sec}^{-1}]$, with 18% of luminosity lost on recombination. With the recombination suppressed by undulators (Fig. I.A.5.8), an average luminosity during 4-hour store becomes $\langle L \rangle = 7 \cdot 10^{27} [\text{cm}^2 \text{sec}^{-1}]$. Also, for the detuning in relative energy introduced by an undulator, agreement between theoretical expression for the recombination coefficient (used in this studies) and experimental measurements is very good [30].

I.A.6 Scenarios of cooling at RHIC: heavy ions

There are various possibilities of using electron cooling at RHIC [6]. Direct cooling at 100 GeV is considered as a base line approach for RHIC-II. However, for eRHIC [31], it is important that cooling is fast enough and sufficient to have the rms beam parameters being cooled substantially, especially the rms bunch length. In such a case, pre-cooling at low energy becomes very attractive due to a strong dependence of the cooling time on energy. For the same reason, cooling is very effective for scenarios with collisions at low energy [6].

Direct cooling of Au ions at storage energy of 100 GeV/n with parameters in Table I.A.5.1 allows us to reach a desired increase in the luminosity ($\langle L \rangle = 7 \cdot 10^{27} [\text{cm}^2 \text{sec}^{-1}]$ during 4-hour store) for the RHIC-II upgrade.

In addition to the luminosity shown in Figs. I.A.5.1 and I.A.5.5, cooling of the rms transverse emittances and rms bunch length are shown in Figs. I.A.6.1-5. Figures I.A.6.1-3 show rough estimates based on the “rms dynamics” approach. In these simulations position of electron bunch is always fixed and its center coincides with the center of the ion bunch. The rms growth rates slightly depend of the length of the electron bunch. Figures I.A.6.1-2 correspond to the situation when longitudinal bunch length of electron beam equals to the one of ions. One can see that with such cooling rates, rms bunch length of ions stays approximately constant while rms transverse emittance of ions is slightly cooled. One can optimize electron bunch length to get more longitudinal cooling which would result is a weak cooling of the bunch length of ions, however, this comes at the expense of the transverse cooling so that there is no noticeable net gain in the luminosity.

Note that the “rms dynamics” approach is used only for a rough estimate of the effects. For more realistic estimate we use the “Modeled beam” approach within the BETACOOOL code. Compared to the “rms dynamics” this method of tracking allows us to see what happens to the ion distribution when the length of the electron beam is varied. Using the “Modeled beam” approach in Figs. I.A.6.4-5, one can see that an rms bunch length of ions is actually increasing, this is due to particles at large amplitudes which are not effectively cooled but which are used in the calculation of the rms parameters of the distribution (see Fig. I.A.6.6-9). This effect is especially pronounced in the longitudinal direction if we use an rms bunch length of the electron beam equal to 1cm (present baseline) while an rms bunch length of the ion beam is around 20cm.

Difference in the ion rms bunch length resulting due to cooling by using the electron bunch with the rms length of 1 cm and 15 cm is shown in Figs. I.A.6.6-9.

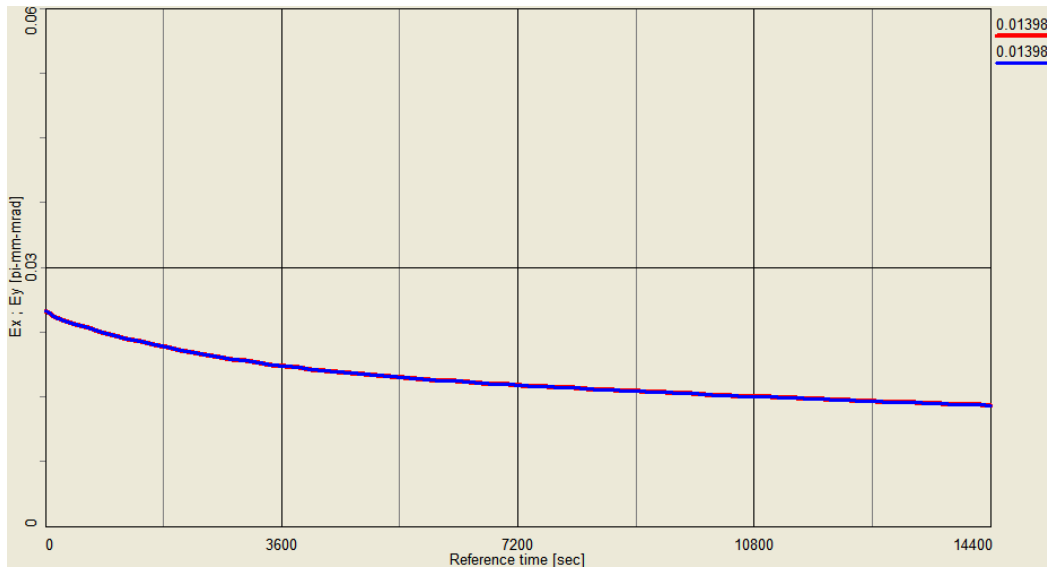


Fig. I.A.6.1 Cooling of horizontal and vertical rms emittances – using “rms dynamics” approach. Plotted emittances are rms unnormalized. Corresponding 95% normalized emittances after 4 hours of cooling are $9.0 \pi \mu\text{m}$ (initial emittance $15 \pi \mu\text{m}$).

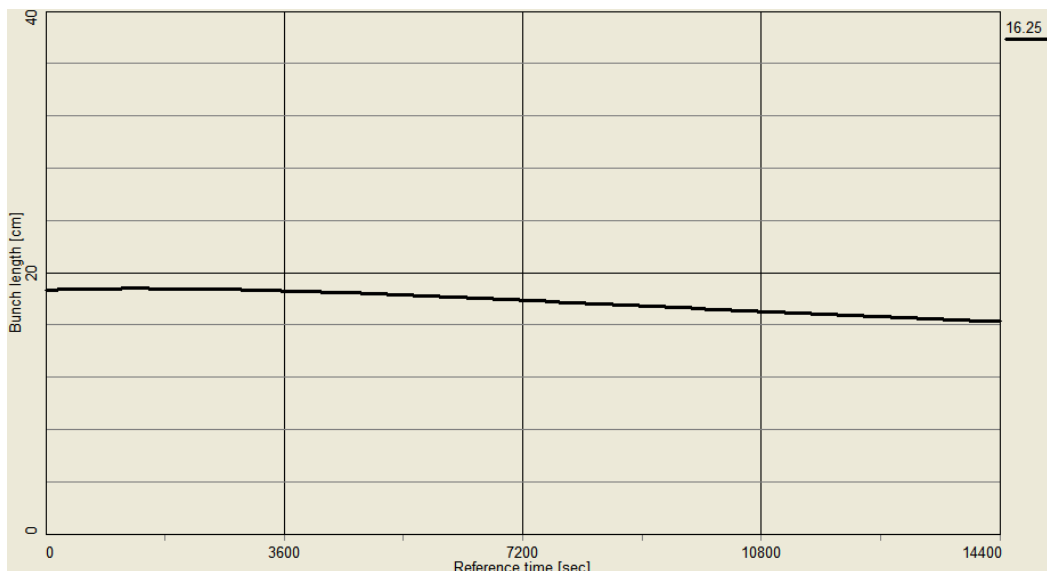


Fig. I.A.6.2 Cooling of rms bunch length – using “rms dynamics” approach, with the ion rms bunch length being cooled to 16 cm after 4 hours (initial length 18cm rms).

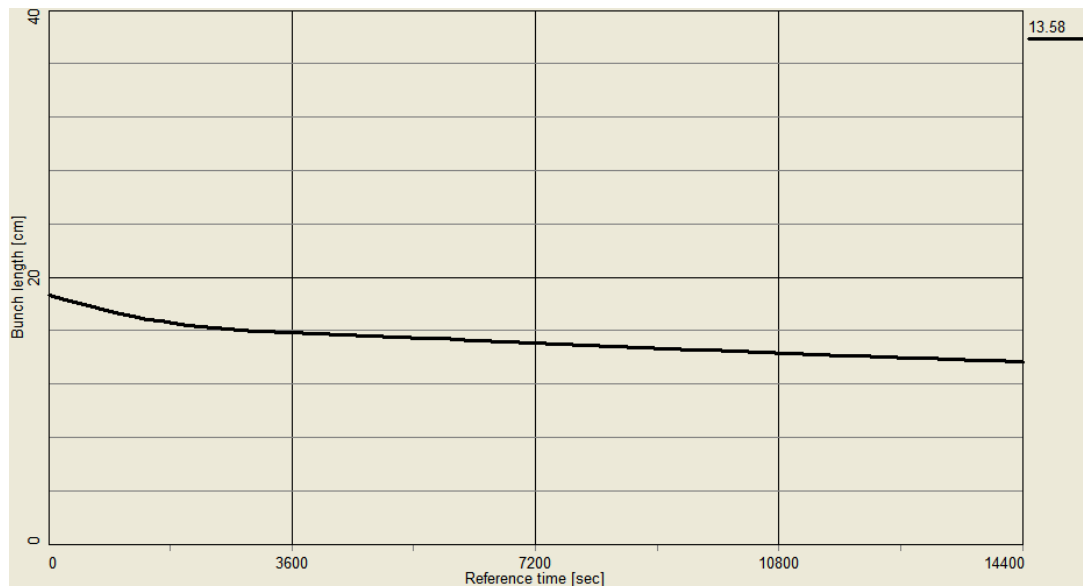


Fig. I.A.6.3 Cooling of rms bunch length – using “rms dynamics” approach, with the ion rms bunch length being cooled to 13.6 cm after 4 hours.

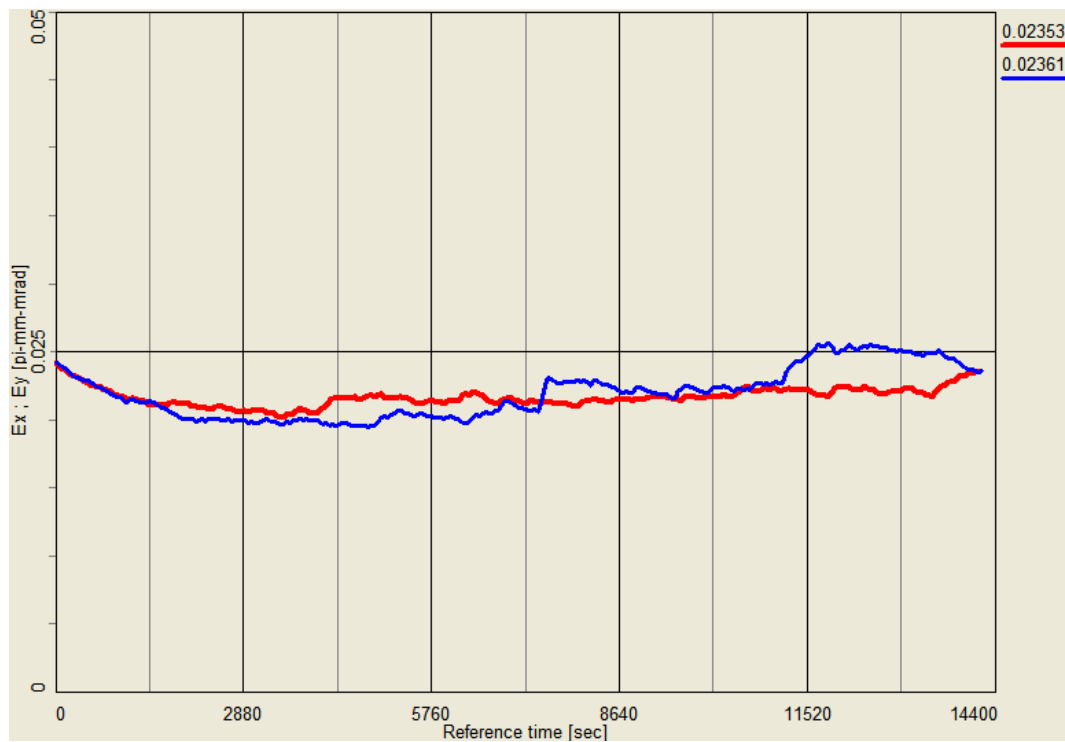


Fig. I.A.6.4 Cooling of horizontal and vertical rms emittances – using “Modeled beam approach”. Plotted emittances are rms unnormalized. Corresponding 95% normalized emittances after 4 hours are $15 \pi \mu\text{m}$.

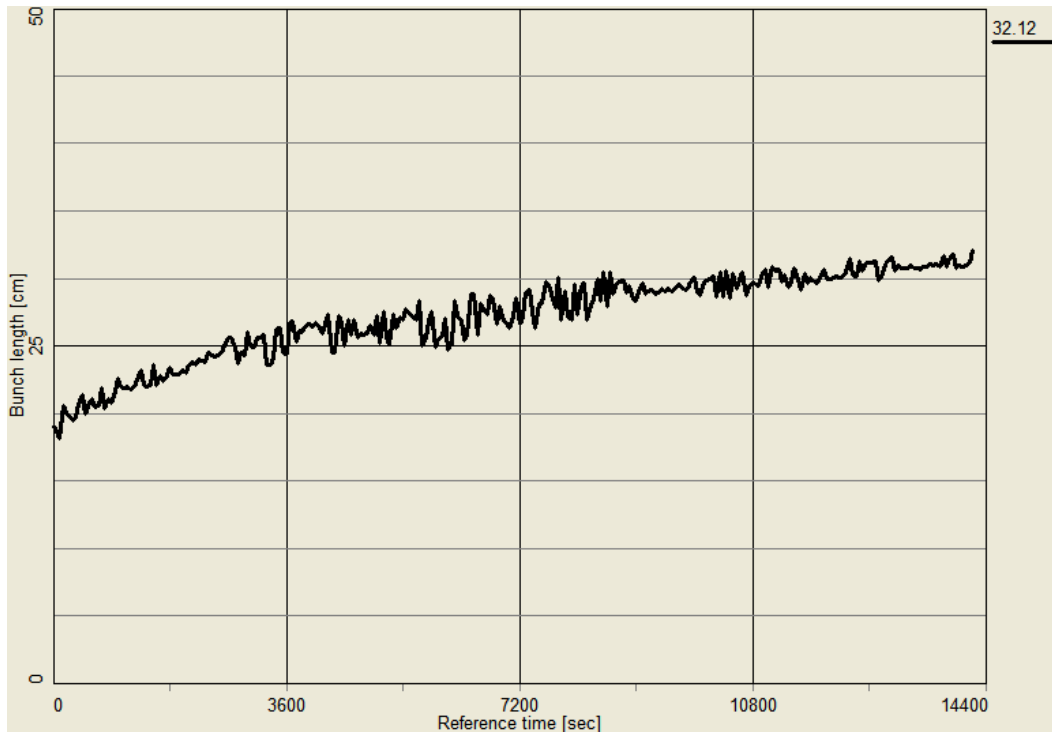


Fig. I.A.6.5 Rms bunch length – using “Modeled beam” approach with 1 cm rms electron bunch. An increase in rms bunch length is due to particles at very large amplitudes.

Figure I.A.6.6 shows 90% bunch length corresponding to Fig. I.A.6.5. One can see that with 1 cm electron bunch sitting in the center of the ion bunch, the 90% bunch length is still increasing. Figure I.A.6.7 shows that more than 10% of the beam in the longitudinal direction is not cooled.

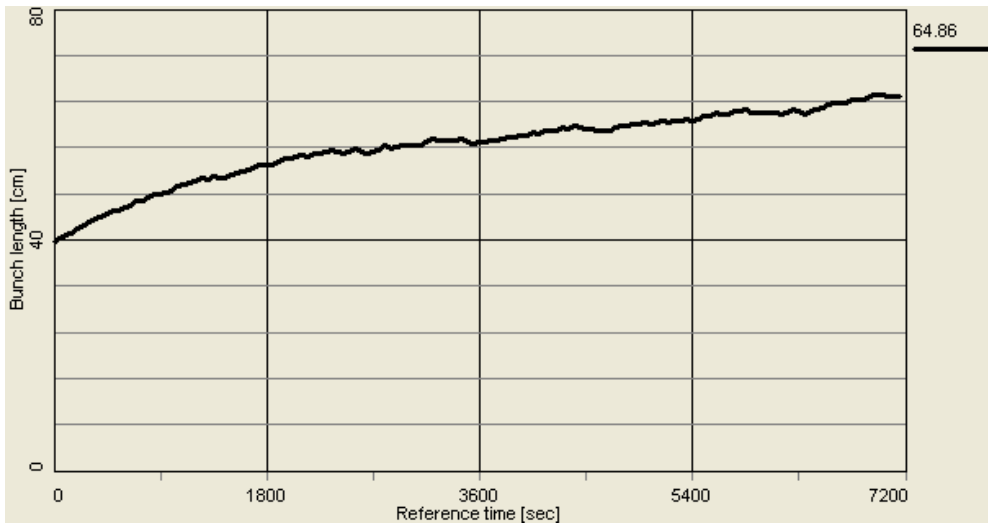


Fig. I.A.6.6 “Modeled beam” approach – 90% bunch length using electron bunch with the rms bunch length of 1 cm.

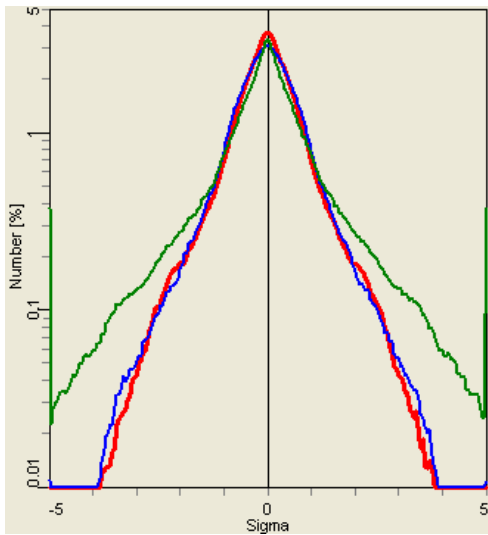


Fig. I.A.6.7 Beam profiles (horizontal: red, vertical: blue, longitudinal: green) after 2 hours of cooling with 1 cm electron rms bunch length.

On the other hand, Fig. I.A.6.8 shows that 90% bunch length is cooled when the electron bunch length is 15 cm rms. Figure I.A.6.9 shows that only 2% of the beam in the longitudinal direction is not cooled in this case.

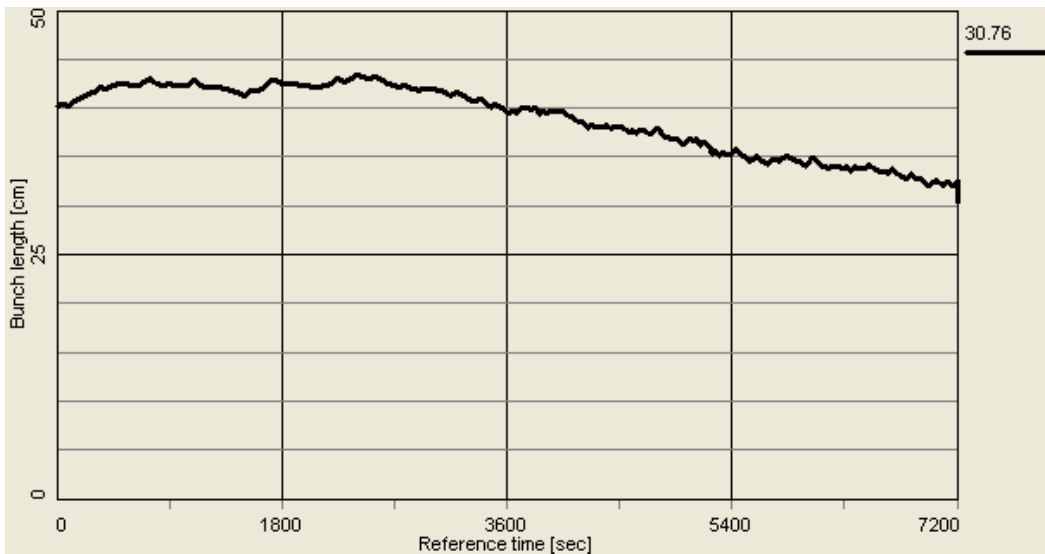


Fig. I.A.6.8 “Modeled beam” approach – 90% bunch length using electron bunch with the rms bunch length of 15 cm.

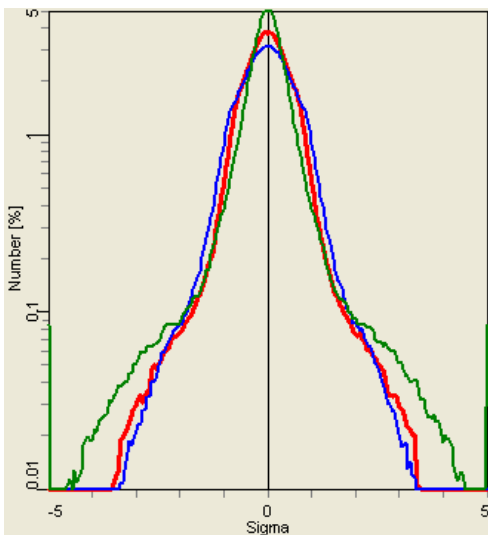


Fig. I.A.6.9 Beam profiles (horizontal: red, vertical: blue, longitudinal: green) after 2 hours of cooling with 15 cm electron rms bunch length.

It can be shown that the longitudinal cooling rate of a long electron bunch with its length approximately equal to the one of ions is identical to the cooling rate of a very short electron bunch which is constantly moved back and forth in the longitudinal direction from the center of ion bunch towards its tails. We refer to such procedure as “painting”.

Painting procedure was tested within the BETACOOOL code where the electron bunch was moved slowly from the longitudinal center of the ion bunch to 2 rms values in the longitudinal direction and back to the center. The resulting longitudinal distribution (green) can be seen in Figs. I.A.6.10 – I.A.6.13. Cooling of the longitudinal tails and stabilization of the ion rms bunch length was clearly observed. Figures I.A.6.14 –I.A.6.15 show resulting rms bunch length and emittance, respectively. In addition, painting with the electron beam allows to avoid additional complication in the electron beam transport system by transporting short bunch.

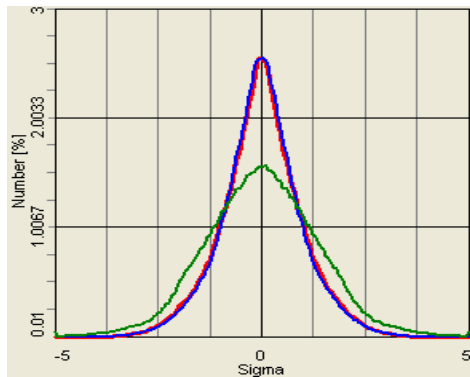


Fig. I.A.6.10 Beam profiles with electron bunch moving towards large amplitudes.

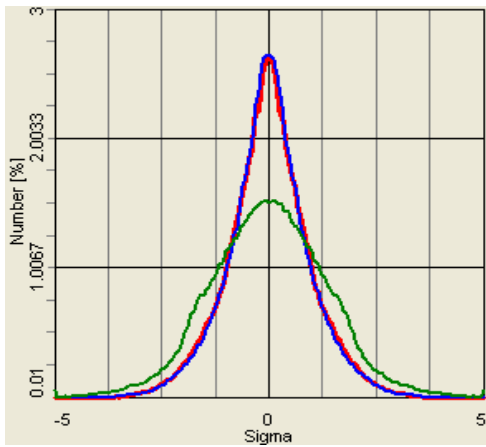


Fig. I.A.6.11 Beam profiles with the electron bunch sitting at 2 rms of the distribution.

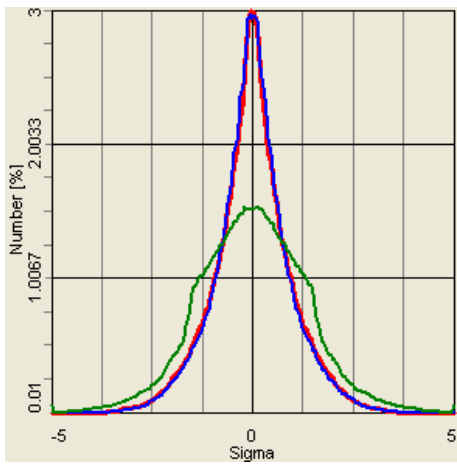


Fig. I.A.6.12 Beam profiles with the electron bunch moving back towards the center.

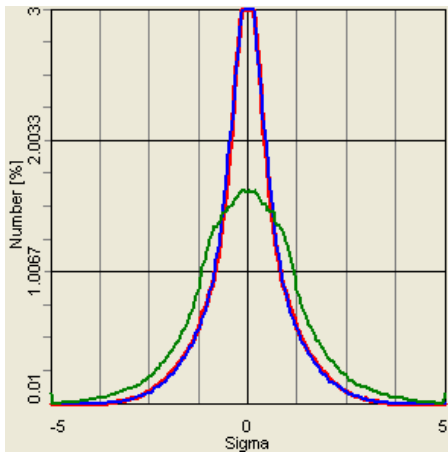


Fig. I.A.6.13 Example of the distribution resulting due to the longitudinal painting.

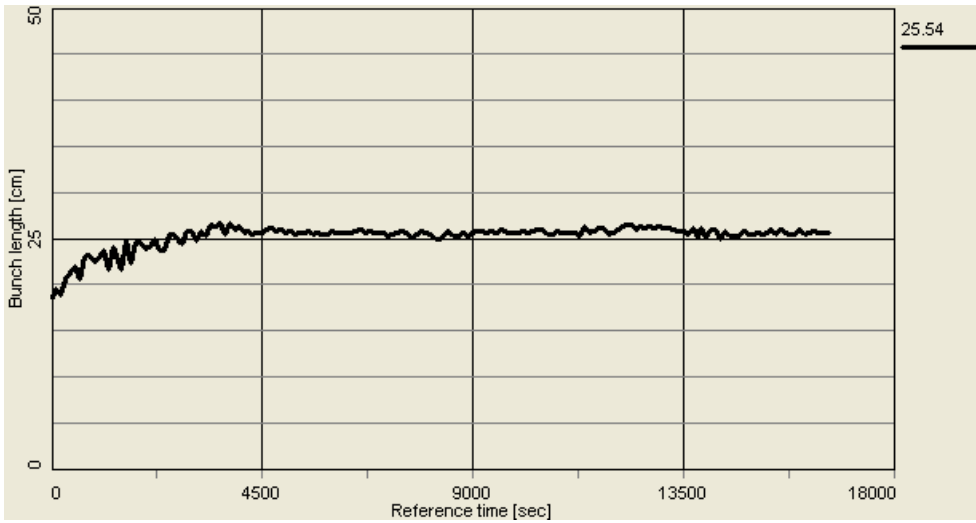


Fig. I.A.6.14 Rms bunch length with painting, using “Modeled beam” approach.

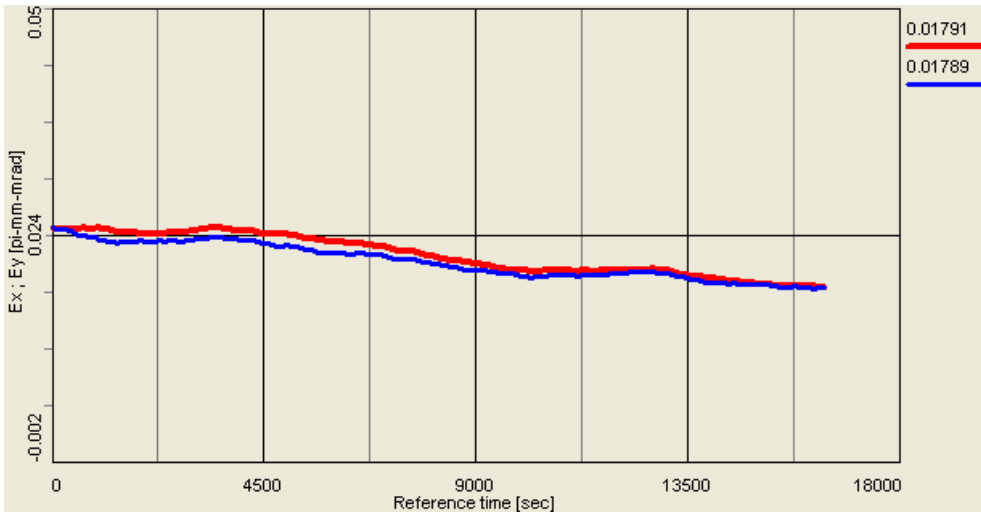


Fig. I.A.6.15 Rms emittance with painting, using “Modeled beam” approach.

With a smooth procedure for painting one can prevent any growth of the rms bunch length, as shown in Fig. I.A.6.16.

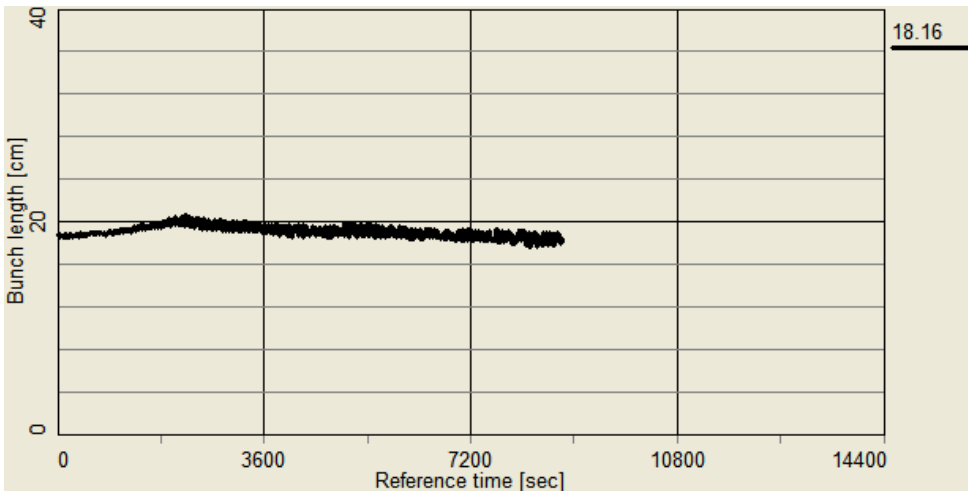


Fig. I.A.6.16 Rms bunch length with painting, using “Modeled beam” approach.

As a result of recent studies, our conclusion is that painting procedure is an effective way to control the longitudinal bunch length of ions. We found that stretching of electron beam is not necessary and that the cooling rates needed can be obtained with a short electron bunch together with a procedure of painting. The rms length of electron bunch is presently given by the transport of the electron beam and is approximately 1 cm.

In addition to painting, the stochastic cooling system, which is presently under development for RHIC, should be very effective in cooling of tails of the distribution.

I.A.7 Scenarios of cooling at RHIC: protons

For protons, the best performance is achieved when protons are first pre-cooled at low energy and cooling is continued either at beam energy of 110 GeV or 250 GeV. Various scenarios for cooling of protons were performed (not discussed here). Here, we just give two examples of performance at 100 and 250 GeV.

For the case of 100 GeV, even without pre-cooling at low energy one obtains promising results. Such a direct cooling at 100 GeV is shown in Figs. I.A.7.1-2 for the rms emittance and bunch length, respectively.

The following parameters were used. Protons: initial 95% normalized emittance $12 \pi \mu\text{m}$, rms radius 4.7mm (beta function 800m), $h=2520$. Electrons: $q=5\text{nC}$, rms emittance $3 \pi \mu\text{m}$, rms radius 5.0mm.

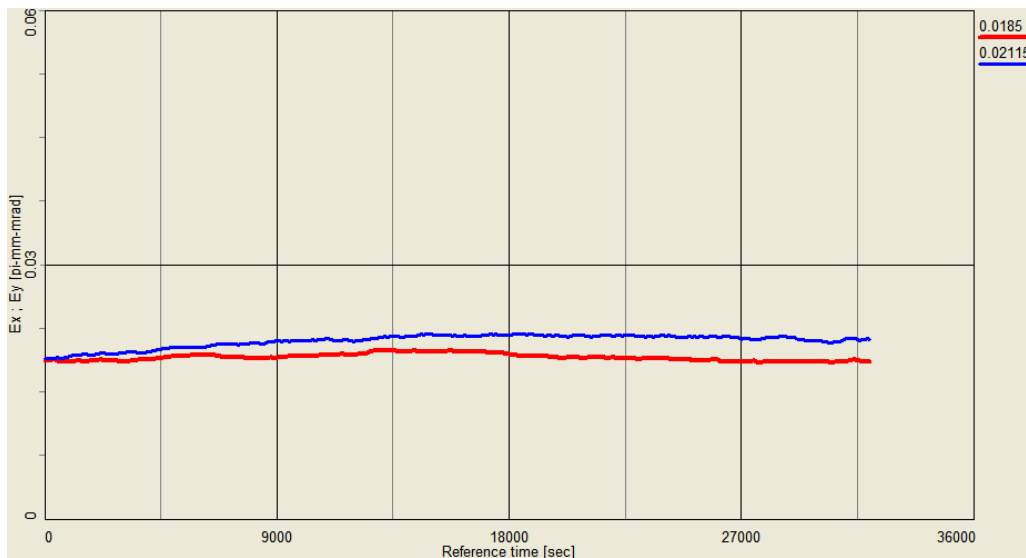


Fig. I.A.7.1 Time evolution of horizontal and vertical rms emittances - cooling of protons at 100 GeV (with initial 95% normalized emittance of $12 \pi \text{ mm mrad}$). Plotted emittances are rms unnormalized.

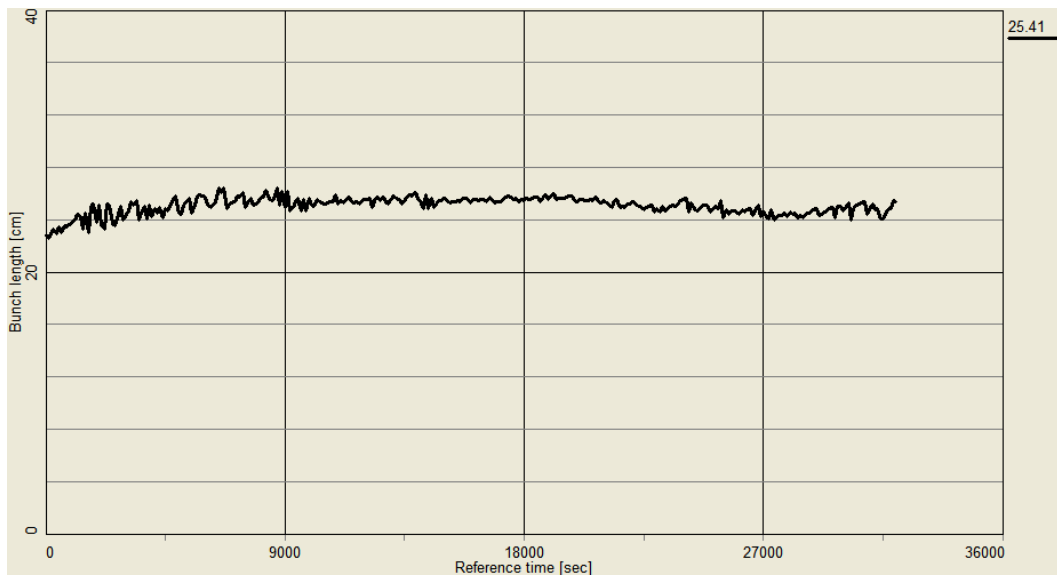


Fig. I.A.7.2 Time evolution of rms bunch length – direct cooling at 100 GeV.

For the top energy of 250GeV, it was found that direct cooling at the top energy with present baseline parameters do not have significant impact on the luminosity. The purpose of electron cooling is thus to pre-cool proton beam at low energy (if needed) and then let emittances grow at the top energy of 250 GeV due to IBS. The resulting luminosities in such approach are equal or higher than the baseline luminosity of RHIC-II.

Figures. I.A.7.3-4 show time evolution of the rms emittance and bunch length, respectively. The following parameters were used. Protons: initial 95% normalized emittance $12 \pi \mu\text{m}$, $h=2520$.

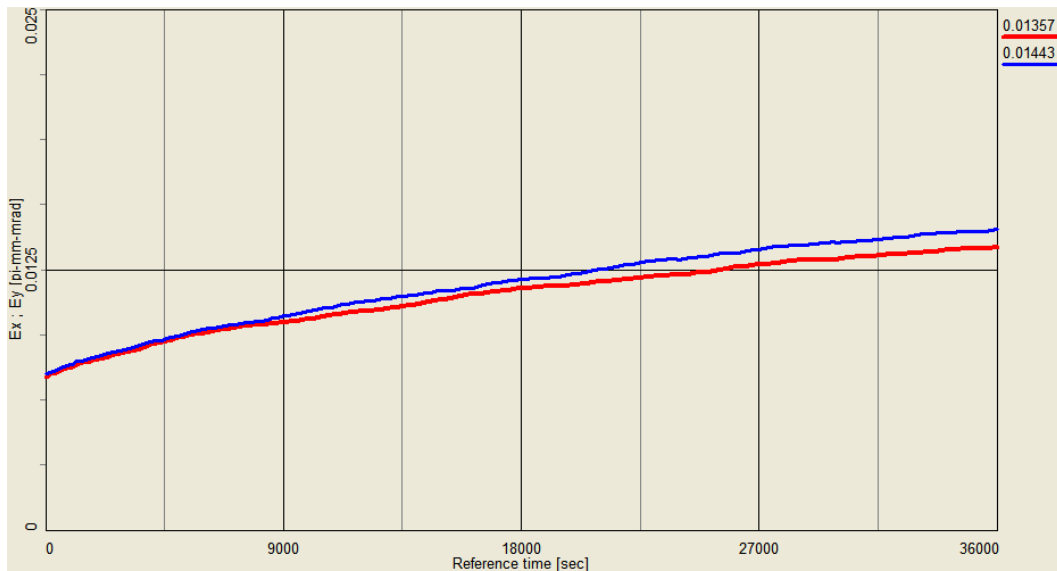


Fig. I.A.7.3 Time evolution of horizontal and vertical rms emittances - protons at 250 GeV. Plotted emittances are rms unnormalized.

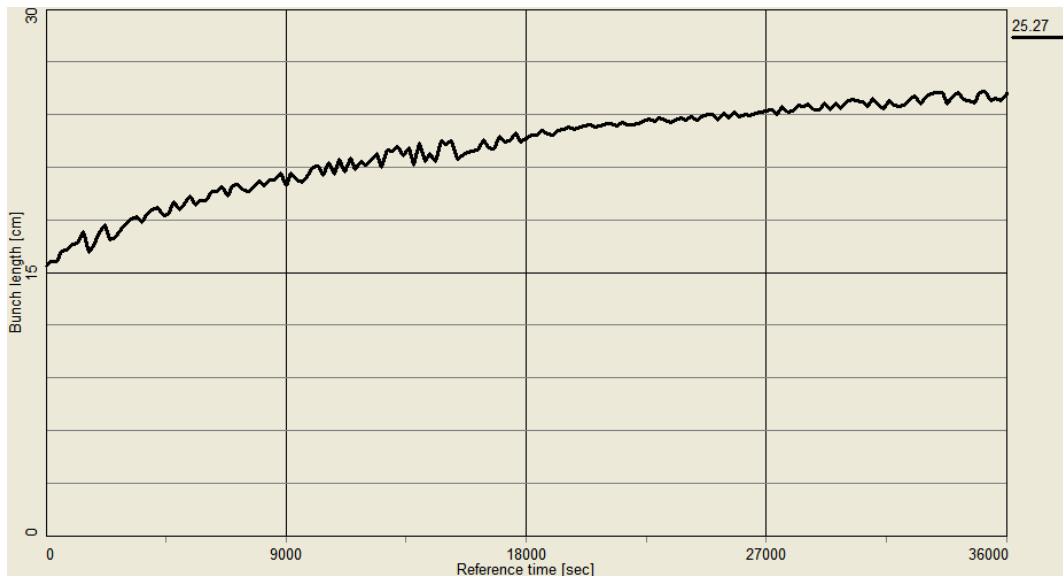


Fig. I.A.7.4 Time evolution of rms bunch length – protons at 250 GeV.

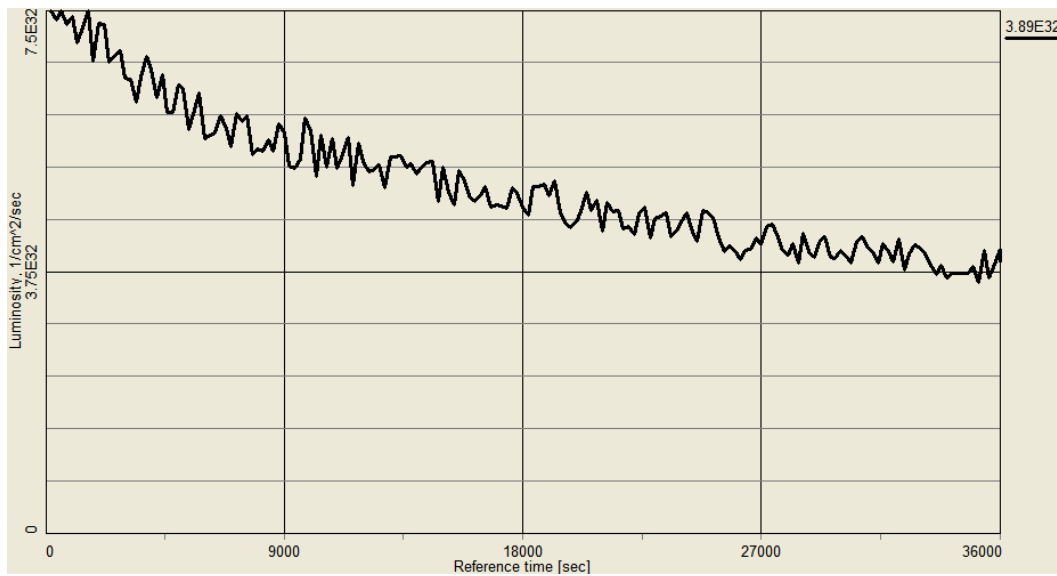


Fig. I.A.7.5 Time evolution of luminosity for protons at 250 GeV.

For parameters used in simulations in Figs. I.A.7.3-5 (112 bunches, $\beta^*=0.5\text{m}$, $N=2e11$) the peak luminosity is $L=7.5 \cdot 10^{32} \text{ [cm}^2\text{sec}^{-1}\text{]}$. The average luminosity during 10-hour store is $\langle L \rangle = 5 \cdot 10^{32} \text{ [cm}^2\text{sec}^{-1}\text{]}$, which are the baseline RHIC-II goals for protons at 250 GeV.

Further increase in proton luminosities is possible by pre-cooling of protons at low energy and/or minimizing initial β^* . Figures. I.A.7.6-9 show time evolution of the rms emittance and bunch length and resulting luminosities for protons at 250 GeV when initial 95% normalized emittance of protons was pre-cooled to $8 \pi \mu\text{m}$ at low-energy. Simulations are then performed at the top energy of 250GeV without cooling.

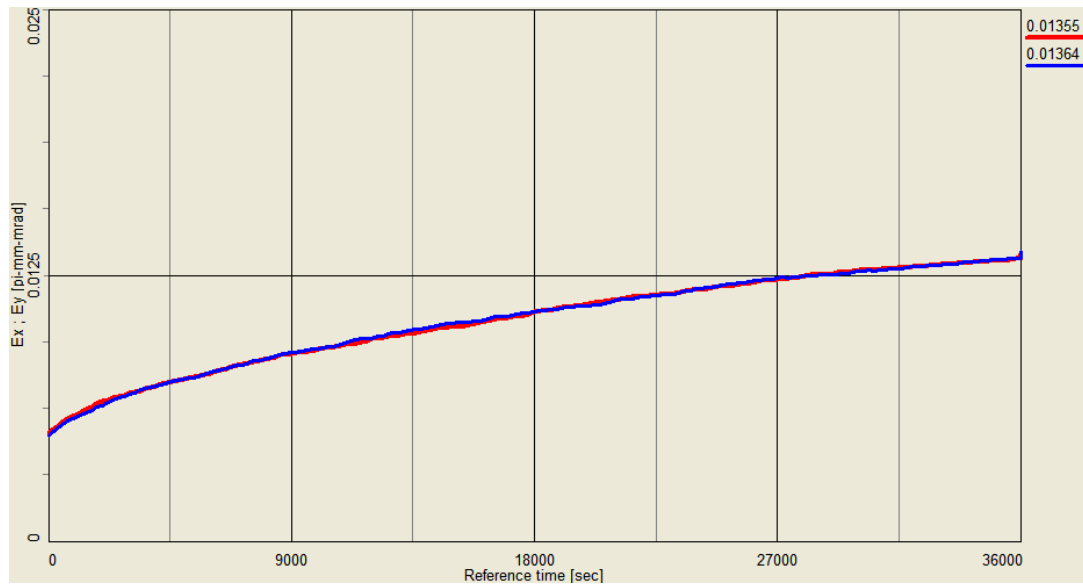


Fig. I.A.7.6 Time evolution of horizontal and vertical rms emittances - protons at 250 GeV with initial 95% normalized emittance of $8 \pi \mu\text{m}$. Plotted emittances are rms unnormalized.

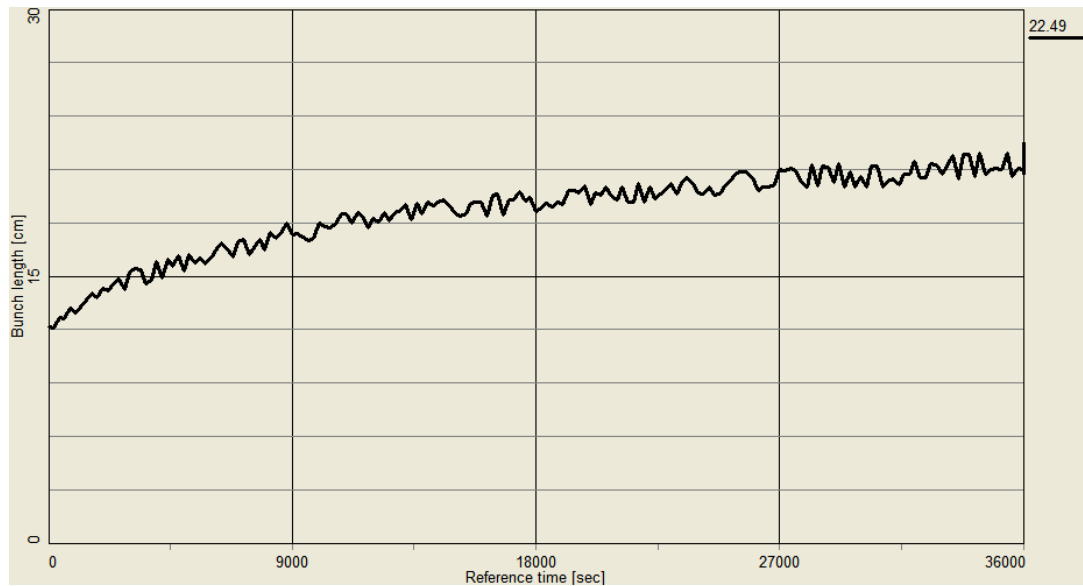


Fig. I.A.7.7 Time evolution of rms bunch length – protons at 250 GeV.

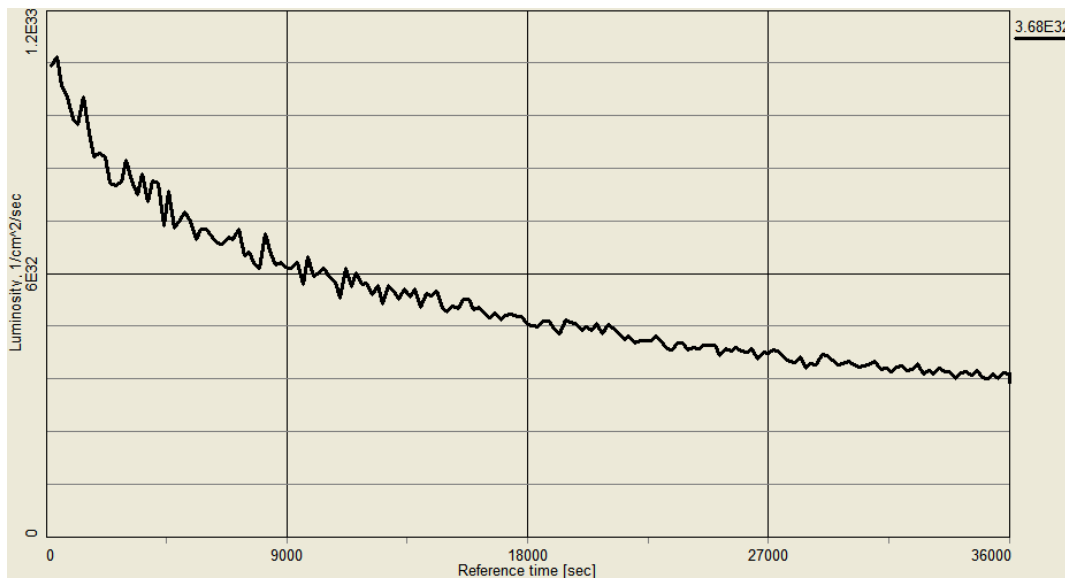


Fig. I.A.7.8 Time evolution of luminosity for protons at 250 GeV (initial emittance 95% normalized emittance of $8 \pi \mu\text{m}$, $\beta^*=0.5\text{m}$).

For parameters in Fig. I.A.7.8 (112 bunches, $\beta^*=0.5\text{m}$, $N=2e11$, initial 95% normalized emittance of $8 \pi \mu\text{m}$) the peak luminosity is $L=1.0 \cdot 10^{33} [\text{cm}^2\text{sec}^{-1}]$. The average luminosity during 6-hour store is $\langle L \rangle = 6.3 \cdot 10^{32} [\text{cm}^2\text{sec}^{-1}]$.

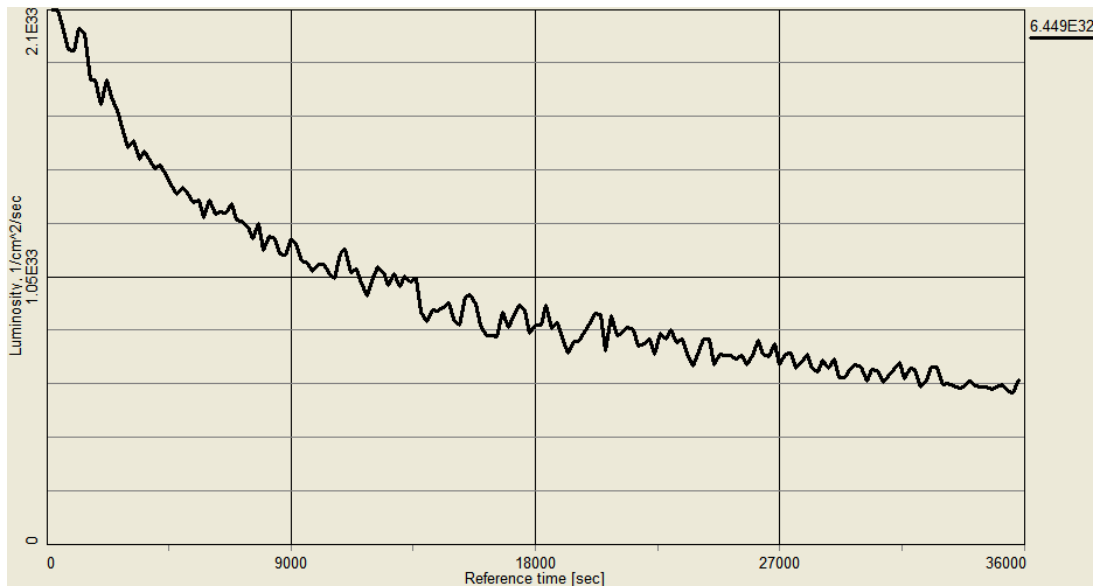


Fig. I.A.7.9 Time evolution of luminosity for protons at 250 GeV (initial emittance 95% normalized emittance of $8 \pi \mu\text{m}$, $\beta^*=0.5\text{m}$)

For parameters in Fig. I.A.7.9 (112 bunches, $\beta^*=0.25\text{m}$, $N=2e11$, initial 95% normalized emittance of $8 \pi \mu\text{m}$) the peak luminosity is $L=2.0 \cdot 10^{33} [\text{cm}^2\text{sec}^{-1}]$. The average luminosity during 10-hour store is $\langle L \rangle = 1 \cdot 10^{33} [\text{cm}^2\text{sec}^{-1}]$.

I.A.8 Luminosity limitations under cooling

I.A.8.1 Incoherent beam-beam effects

The electro-magnetic force field of a moving bunch produces a force which acts on individual particles in another bunch moving in the opposite direction. Such a force acting on individual particles is referred to as incoherent beam-beam force. One can integrate this force over the collision to obtain the incoherent beam-beam kick.

Beam-beam kick for head-on collision

One typically starts consideration of beam-beam effects with calculation of an increment of transverse particle momentum change after crossing the encounter bunch, considering "strong-weak" approximation of beam-beam interaction. In this model it is assumed that particles of the weak-beam (index 2) are influenced by a strong electromagnetic field of the opposite bunch (index 1), while the strong bunch does not feel any field of the weak bunch.

The change of slope of particle trajectory in linear approximation can be written as follows:

$$\Delta \frac{dx}{ds} = \frac{\Delta p_x}{p_s} = 4\pi \frac{\xi_x}{\beta_x^*} x, \quad \Delta \frac{dy}{ds} = \frac{\Delta p_y}{p_s} = 4\pi \frac{\xi_y}{\beta_y^*} y, \quad (\text{I.A.8.1})$$

where ξ_x, ξ_y are beam-beam parameters, which have a meaning of linear part of betatron tune shift due to beam-beam collision:

$$\xi_x = N_1 \frac{\beta_x^*}{4\pi} \frac{q_1 q_2}{4\pi\epsilon_0 m_2 c^2} \frac{(1 + \beta_1 \beta_2)}{\gamma_2 \beta_2 (\beta_1 + \beta_2)} \frac{2}{\sigma_x (\sigma_x + \sigma_z)}, \quad (\text{I.A.8.2})$$

$$\xi_y = N_1 \frac{\beta_y^*}{4\pi} \frac{q_1 q_2}{4\pi\epsilon_0 m_2 c^2} \frac{(1 + \beta_1 \beta_2)}{\gamma_2 \beta_2 (\beta_1 + \beta_2)} \frac{2}{\sigma_z (\sigma_x + \sigma_z)}. \quad (\text{I.A.8.3})$$

Here, the values of beta-function at the interaction point are β_x^*, β_y^*

For collisions of the particles at equal velocities ($\beta_1 = \beta_2 = \beta$), charge numbers ($q_1 = q_2 = Z$) and atomic numbers the beam-beam parameters can be simplified:

$$\xi_x = \frac{\beta^*}{4\pi} \frac{Z^2}{A} r_p \frac{N(1 + \beta^2)}{\beta^2 \gamma \sigma_x (\sigma_x + \sigma_z)}, \quad (\text{I.A.8.4})$$

$$\xi_z = \frac{\beta^*}{4\pi} \frac{Z^2}{A} r_p \frac{N(1 + \beta^2)}{\beta^2 \gamma \sigma_z (\sigma_x + \sigma_z)}. \quad (\text{I.A.8.5})$$

For the relativistic factor $\beta=1$ one has

$$\xi = \frac{\beta^* Z^2}{2\pi A} r_p \frac{N}{\gamma \sigma_z (\sigma_x + \sigma_z)} \quad (\text{I.A.8.6})$$

Stability of linear incoherent motion

In the linear approximation, the motion of a test particle in the presence of the other beam is stable if the absolute value of the trace of the one-turn transfer matrix is less than 2.

Such stability criteria gives very large attainable linear beam-beam tune shifts, which indicates that much smaller experimentally achieved beam-beam parameters are not due to this stability mechanism.

I.A.8.2 Coherent beam-beam effects

Coherent beam-beam effects arise from the forces which an exciting bunch exerts on a whole test bunch during collision. The corresponding coherent kick is obtained by integrating incoherent beam-beam kick over the charge distribution of the test bunch. In ideal case, due to a symmetry, the coherent beam-beam kick vanishes for head-on collisions.

Linear tune shift

The linear coherent beam-beam tune shift can be calculated and becomes just one half of the linear incoherent shift ξ :

$$\Xi = \frac{\beta^* Z^2}{4\pi A} r_p \frac{N}{\gamma \sigma_x (\sigma_x + \sigma_z)} \quad (\text{I.A.8.7})$$

Stability of linear coherent motion

Coherent oscillation of two beam under certain condition can lead to an instability. With one bunch per beam to modes are possible, the 0-mode, where both beam oscillate in phase and π -mode where both beam oscillate out of phase. With m bunches per beam, one gets $2m$ modes of oscillation, correspondingly.

The stability of the system can be also calculated in the linear matrix theory. Although the threshold is now significantly lower then in the incoherent case it is still well above the experimentally observed beam-beam limits.

I.A.8.3 Nonlinear effects and beam-beam limit

Non-linear tune spread and resonances

The nonlinear variation of the beam-beam force with radius in a round Gaussian beam causes a tune shift of individual particles to have dependence on particle oscillation amplitude. For the distribution of particles within the beam this results in a tune-spread in the beam. In addition the beam-beam force drives non-linear resonances.

Experimental beam-beam limit is usually attributed to excitation of non-linear resonances. Overlapping of resonances results in stochastic particles motion with corresponding particle loss. The strength of nonlinear beam-beam resonances can be related to the incoherent beam-beam parameter which allows to use its value to describe beam-beam limit. In principle, an estimate of the real beam-beam limit should include nonlinear resonances excited by the magnet imperfections which then makes beam-beam limit to be machine dependent.

In lepton machines, the beam-beam tune spread is much high than in hadron machine. As a result, many nonlinear resonances are crossed. However, diffusion caused by a very high-order nonlinear resonance is compensated by intrinsic damping mechanism of lepton machines which is the synchrotron radiation.

In the absence of damping mechanism diffusion even by a very high-order resonances can have significant effect on particles losses, which is believed to be the case for hadron machine. Introduction of additional fast damping mechanism, such as e-cooling can offset diffusion due to high-order resonance, at least partially, and thus lead to higher values of beam-beam parameters. Due to a very slow cooling rates at high energy, this damping mechanism may not lead to compensation of beam-beam diffusion. However, this question of equilibrium between beam-beam and cooling requires very careful computational study, especially for non-Gaussian distributions which may appear as a result of cooling.

I.A.8.4 Beam-beam simulations for ion beam under cooling

It is extremely important to treat beam-beam effects for the ion beam while the cooling is present. The main purpose of cooling is to counteract diffusion of ion beam which may be caused by various effects. For accurate treatment, dynamic simulation code should include both cooling and diffusion sources, including intrabeam scattering and beam-beam diffusion. As a simple model, one can describe beam-beam effects with a diffusion coefficient, based on beam-beam space-charge force. Such a coefficient, either approximate analytic or empiric (based on real measurements in RHIC) can be used in dynamic simulation code. Simulations of beam cooling including beam-beam diffusion are planned in the future.

As a result of beam-beam force one has two major effects: excitation of beam-beam resonances and tune spread. Because of the tune spread many non-linear imperfection resonances can be crossed which results in a significant beam diffusion and in so called empiric beam-beam limit. A reliable way to account for beam-beam effects and to have a reasonable description of achievable beam-beam limit is to include non-linear optics of the machine (imperfection resonance) into account. Such simulations of beam-beam effects and cooling are planned in the framework of UAL

simulation [32]. In addition, the UAL based simulation should describe both incoherent and coherent effects in a self-consistent manner.

Presently, simulations of electron cooling are done without taking into account beam-beam diffusions. As a guideline we only use the values of the beam-beam parameter which is calculated from the local density when the “Model beam” approach is being used.

As an example, Figs. I.A.8.1 and I.A.8.2 show the beam-beam parameter for the cooling simulations in Fig. I.A.5.1 and parameters in Table I.A.5.1, using the “rms dynamics” and “Model beam” approach, respectively.

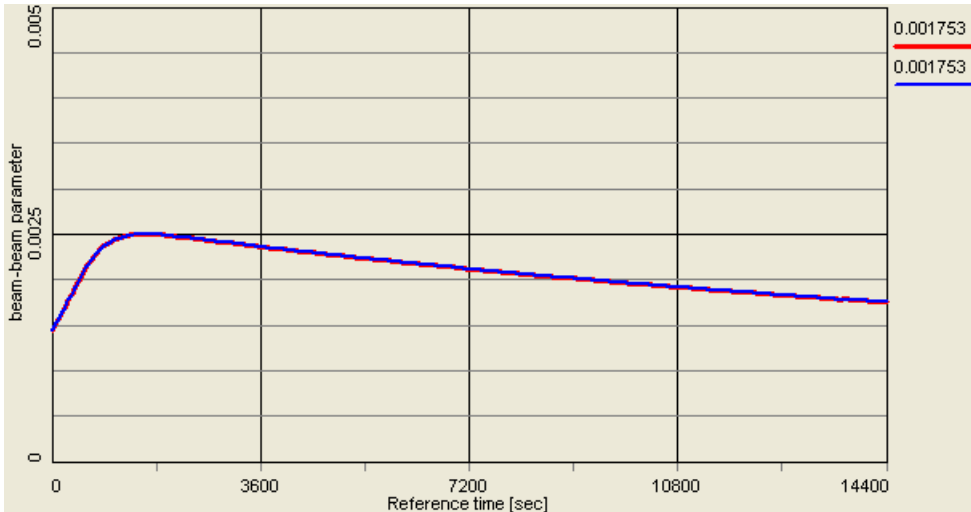


Fig. I.A.8.1 Resulting beam-beam parameter for parameters in Table I.A.5.1, calculated using rms dynamics approach.

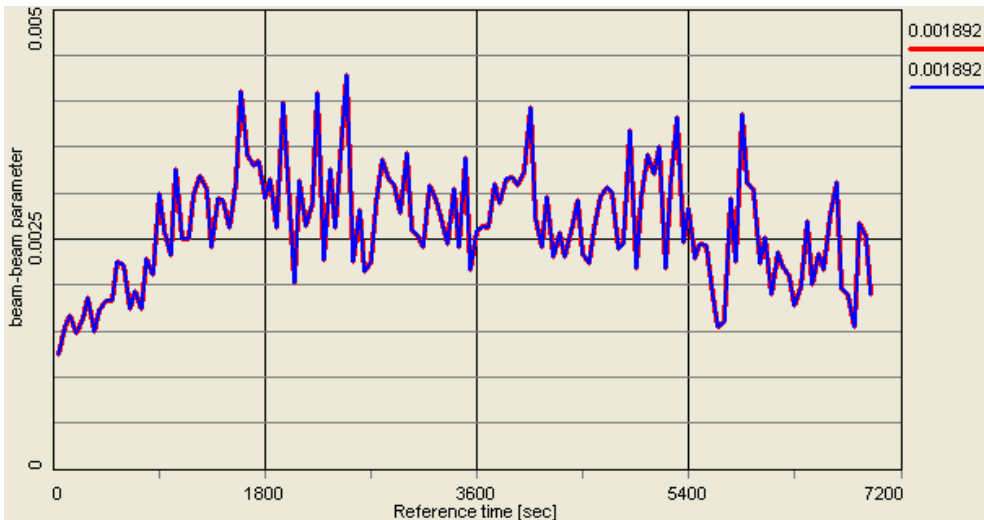


Fig. I.A.8.2 Resulting beam-beam parameter for parameters in Table I.A.5.1, calculated via local density using “Model beam” approach (oscillations are due to the numerical noise).

I.A.9 Effects on electron beam

For RHIC one needs to cool ion beams in two rings (yellow and blue). The present approach is to use a single ERL and the same electron beam to cool the ion bunch in both rings, which requires to use each electron bunch for cooling twice. An alternative approach (with an increase of electron beam current) is to adjust timing/return path in a way that each electron bunch interacts only once with the ion beam.

Independently of the approach chosen, to ensure good cooling performance a quality of the electron beam should not suffer significantly as a result of the electron beam transport, merging of the electron and ion beam, and interactions with the ion beam.

An increase in the electron emittance (transverse angular spread) and longitudinal momentum spread was estimated due to the following effects:

1) Intra-beam scattering within the electron beam

For present parameters of electron beam, the longitudinal rms velocity spread of electrons in the beam frame is smaller than transverse. The transverse-longitudinal relaxation due to IBS results in an increase of the longitudinal rms velocity spread. A relative fractional increase in the longitudinal rms velocity spread after 100 meters was found to be at 10^{-4} level, which is considered to be negligible.

2) Intra-beam scattering between the electron and ion beam.

A relative increase in the longitudinal rms velocity spread was found to be less than 1% as a result of 100 meters of interaction with the ion beam, which is considered to be negligible.

3) Coherent Synchrotron Radiation (CSR) radiation

The rms energy spread and the average energy loss, ignoring vacuum chamber shielding, can be estimated from the following expressions:

$$\sigma_E = 0.25 \frac{r_e N_e L_{eff}}{\gamma (R^2 \sigma_{es}^4)^{1/3}} \quad (\text{I.A.9.1})$$

where L_{eff} is total effective length of bending path, R is the bending radius, σ_{es} is the rms length of the bunch, N_e is number of electron per bunch and r_e is the classical radius of electron.

$$\langle E \rangle = -0.35 \frac{r_e N_e L_{eff}}{\gamma (R^2 \sigma_{es}^4)^{1/3}} \quad (\text{I.A.9.2})$$

Taking typical parameters of electron beam transport of the system one gets about $\sigma_E=0.001$ and $\langle E \rangle = -0.0014$.

Such an estimate for the rms energy spread is higher than the requirement for cooling < 0.0005 . The energy loss is also at 10^{-3} level which would require compensation with additional rf cavities.

However, the CSR could be shielded by the presence of the beam pipe walls. For an estimate of the shielding effect one can look at the threshold parameter [33]:

$$x_{th} = \frac{2\pi^3 R \sigma_{es}^2}{(3h^3)} \quad (\text{I.A.9.3})$$

where h is the width of the vacuum chamber in the dipole magnet and R is the bending radius of the magnet.

When $x_{th} \ll 1$, one can use unshielded formulas. For $x_{th} > 4\pi^2$, there is no more coherent radiation. In the range $1 < x < 4\pi^2$, the radiation is significantly reduced by a factor $F_r = x_{th}^{-1/3} \exp(-x_{th})$. For the parameters of electron cooler with $R=0.5\text{m}$ and $h=0.03\text{m}$ in the bending magnet we get $x_{th}=38$, which means that CSR in our case is completely suppressed by shielding effect.

Although the estimates presented above suggest that CSR effects will be suppressed, a more accurate estimate of CSR for a realistic design (radius of the curvature, path length) may be needed via computer simulations, including effects of screening due to the beam-pipe wall.

4) Space-charge defocusing due to self fields in the cooling section

The space-charge effect due to self fields gives a significant effect on angular spread. For the linear part of the space-charge defocusing force $F = \Delta k \cdot x$, we have

$$\Delta k_{e,sc} = \frac{2N_e r_e}{\beta^2 \gamma^3 a_e^2 l_{es}} \quad (\text{I.A.9.4})$$

where a_e is radius of electron bunch and l_{es} is the full bunch length. Taking $N_e = 3.121 \cdot 10^{10}$, $a_e = 1\text{cm}$, $l_{es} = 3\text{cm}$ and length of cooling section 100m , corresponding defocusing length $f_{sc} = 200\text{m}$. Such small defocusing length results in angular spread $\theta_{sc} = a_e / f_{sc} = 5 \cdot 10^{-5}$, which is 5 times bigger than required by cooling. This is the upper limit estimate, since the numbers are given in the assumption of constant beam size, although the size would grow by about 50% by the end of cooling section.

To compensate for this space-charge defocusing, the cooling section will have modules of compensating solenoids put in pairs (with opposite magnetic field) every 10 meters.

To compensate this space-charge defocusing with the length $L_s = 0.2\text{m}$ of each of the modules of solenoids, one needs magnetic field of $B_s = 160\text{G}$, which gives focusing length of $F_s = 2000\text{m}$. Each solenoid in the pair presently has magnetic length 0.1m , $R = 5\text{cm}$ and magnetic field B about 200-300G.

5) Space-charge defocusing due to image effects

For relativistic beams, one also needs to consider contribution from wall images, which may dominate over the contribution of the self fields in free space. For RHIC parameters, this would be the case if electron beam would be a dc beam with magnetic field penetrating the walls of the vacuum chamber (and thus no cancellation between electric and magnetic fields as for the self fields in the free space). However, for the short electron bunch in the case of RHIC cooler the fields of interest are not-penetrating. The resulting contribution of wall images into incoherent and coherent wavelength of electron oscillation (space-charge defocusing) is suppressed by an additional $1/\gamma^2$ as for the case of the self fields in the free space.

For the case of cylindrical beam pipe with azimuthal symmetry and symmetric beam on axis the incoherent effect on individual particles vanishes due to symmetry. For the beam centroid displaced from the pipe center by a distance x_c the contribution of images does not cancel and one has $F_c = \Delta k_c \cdot x_c$, where

$$\Delta k_{c,ac} = \frac{2N_e r_e}{\beta^2 \gamma^3 a_e^2 l_{es}} \frac{a_e^2}{b^2} \quad (\text{I.A.9.5})$$

where b is the radius of beam-pipe.

The beam centroid x_c will then be displaced as $x_0 \cosh(s/\lambda_{ac})$, where $\lambda_{ac} = (\Delta k_{c,ac})^{-1/2}$.

With radius of the vacuum chamber in the cooling section $b=5\text{cm}$, we get corresponding defocusing wavelength $\lambda_{ac}=720\text{m}$, which is negligible

For the estimate of the dc contribution one needs to use an average current of the electron beam and the fact that there is no $1/\gamma^2$ reduction for the force anymore. Corresponding defocusing strength is then $\Delta k_{c,dc} = \Delta k_{c,ac} \cdot B_f \gamma^2$, where B_f is the ratio of average to peak current. Taking $B_f=0.001$ we get $\lambda_{c,dc}=200\text{m}$, which gives a noticeable effect in the deflection of beam centroid (about 12% by the end of the cooler). It also sets requirement on the allowed displacement of electron beam in the cooling section in order to keep angles to a required level, which is about 2 mm.

6) Effect of trapped ions

The effect of charge neutralization is also of a concern. The electron beam produces ions by ionization of the residual gas in the vacuum chamber. These ions are easily accumulated. The electric field of these ions has an effect on the electron beam γ^2 times greater than the beam's space charge defocusing effect in Eq. (I.A.9.4). The resulting contribution to transverse angles can be estimated by multiplying angles due to self fields by $(\alpha \gamma^2)$, where α is the neutralization factor $\alpha = n_{si}/n_e$, with n_{si} being the density of secondary ions and n_e being the density of electron.

Although in the case of RHIC a very small neutralization factor can be expected due to a very large distance between the electron bunches (ratio of the electron bunch length to the distance between bunches is about 0.001), this effect becomes important at high energies with $\gamma=107$. In the cooling

section there is no trapped ions since the charge of the ion beam is larger than the one of the electron beam but ion trapping becomes a problem in the transport channel of the electron beam.

To avoid the space-charge neutralization, the ions need to be cleared from the beam. Several options are presently being considered. Also, the estimates were done for needed variation in electron charge in order to produce effective cleaning time, as well as the length of the electron bunch train [34].

7) Collective interactions with beam-pipe wall

Effect of coupling impedances on electron beam was estimated by E. Pozdeyev [35]. The contribution from the resistive-wall wakes, accelerating cavities and bellows was considered.

Contribution to the longitudinal rms energy spread from resistive wake was found to be about $3 \cdot 10^{-5}$ which is about 10% effect. Contribution from the bellows: $5 \cdot 10^{-7}$, which is negligible.

Largest contribution to the longitudinal rms energy spread was estimated to be from accelerator cavities: $4 \cdot 10^{-4}$, which is comparable with the requirement on energy spread needed for cooling, and thus will need to be corrected.

All contributions to the transverse angles of the electron beam from the transverse wakes were found to be negligible.

I.A.10 Effects on ion beam dynamics

I.A.10.1 Tune shifts

1) Incoherent space-charge tune shift within the ion beam

For an ion beam with Gaussian distribution one has

$$\Delta Q_{SC} = \frac{Z^2 N_i r_p C_r}{4\pi A \beta^2 \gamma^2 \epsilon_{in} \sigma_{is} \sqrt{2\pi}} \quad (\text{I.A.10.1})$$

where C_r is ring circumference, ϵ_{in} is the normalized rms emittance and σ_{is} the rms bunch length.

For typical parameters of Au ion beam at 100 GeV one gets ΔQ_{sc} about 0.001.

2) Incoherent tune shift of ions due to interaction with electrons

Electron beam also acts like a focusing lens on positive Au ions which produces an additional tune shift of ion particles:

$$\Delta Q_e = \frac{Z n_e r_p l_c \beta_i}{2 A \beta^2 \gamma^3} \quad (\text{I.A.10.2})$$

where l_c is the length of the cooling section, n_e is the density of electron beam in the laboratory frame and β_i is the average beta-function in the cooling section.

For baseline cooler parameter ΔQ_e is about $8 \cdot 10^{-5}$.

I.A.10.2 Coherent ion-electron interactions

A simple description of such interaction can be done via the model of two oscillators [36]. Even with such simple model, for typical parameters of low-energy cooler, one can obtain that for a very high electron densities and long cooling section the net effect of ion-electron interaction can result in “heating” of the ion beam rather than cooling.

Approximate models were developed in Refs. [36, 37, 38] which allow us to estimate thresholds of this type of instabilities for RHIC parameters. The thresholds of these instabilities were calculated by G. Wang, and showed that for proposed density of the electron beam, the ion beam will remain stable both in the transverse and longitudinal directions. More details on these estimates for RHIC parameters can be found in a separate report [39].

I.A.10.3 Collective instabilities for ion distribution under cooling

A careful study of collective instabilities becomes an important issue for ion beam under cooling at least for two reason:

- tune spread and momentum spread decreases which may result in insufficient Landau damping
- direct space-charge field increases as the beam cools down with a formation of dense core.

The situation is expected to be less critical for present parameter of RHIC cooler, since with present parameters transverse and longitudinal emittances of ions are cooled only slightly, as well as distributions under cooling do not produce dense cores as for the case of the magnetized cooling approach. However, simulation with the realistic RHIC environment are planned in the future to explore this issue in detail.

Requirements on coupling impedance after cooling

For the longitudinal stability a rough condition is

$$\left| \frac{Z}{n} \right| \leq F_L \frac{A}{Z_i^2} \frac{\beta^2 \gamma (m_p c^2 / e) |\eta|}{I_0} \left(\frac{\Delta p}{p} \right)_{FWHM}^2 \quad (\text{I.A.10.3})$$

where the longitudinal form factor depends on the distribution and approximately $F_L=1$. Here, I_0 is the average ion beam current for a coasting beam. For a bunched beam, one can roughly use the local peak current $I_p=eZ_i\beta c/l_b$.

For low-energy cooling, cooling above transition becomes a problem due to the space-charge contribution to the impedance which results in a significant tune shift. For RHIC energies, the space-charge impedance is negligible so that stability will be simply governed by a degree of a collapse of momentum spread $\Delta p/p$. The process of cooling should be carefully controlled to avoid large decrease in $\Delta p/p$.

For the transverse stability, the requirement on the transverse impedance is given by

$$Z_t \leq 4F_T \frac{A}{Z_i^2} \frac{\gamma(mc^2/e)}{I_0} \frac{Q}{R} (\Delta Q)_{FWHM} \quad (\text{I.A.10.4})$$

where full tune-spread ΔQ_{FWHM} is given by

$$(\Delta Q)_{FWHM} = \left[\left((n-Q)\eta + Q'(\Delta p/p) \right)^2 + \left(\left(\partial^2 Q / \partial a^2 \right) a^2 \right)^2 \right]^{1/2} \quad (\text{I.A.10.5})$$

The first term in Eq. (I.A.10.3) is due to the revolution frequency, the second term is due to chromaticity Q' and the third term is due to the nonlinear tune spread with octupoles.

A study of the longitudinal and transverse stability of cooled ion beam in RHIC, with the beam distribution resulting due to cooling will be done in the future.

I.A.10.4 Effect of cooling on polarization of protons

The two effects which may cause depolarization of the circulating ions by the electron cooler are:

- 1) Spin precession in the longitudinal magnetic field B of the solenoid in cooling section.
- 2) Hyperfine interactions (hf) with the cooler electrons.

For typical parameters of a low-energy cooler with strong magnetic field in the solenoid, the spin precession angle caused by this field is very large. However, this effect is easily compensated by additional solenoids with opposite field directions. For the present parameters of RHIC cooling section, compensating solenoid pairs consist of the magnets with opposite field directions.

Theoretical estimates of hf effects were done for typical parameters of low-energy cooler. The depolarization times found suggest that this effect is completely negligible.

Experiments with polarized protons were done in circular accelerators equipped with electron coolers, such as IUCF (Indiana, USA) and COSY (Juelich, Germany). No effects on polarization of protons as a result of the electron cooler was observed [40].

I.A.11 REFERENCES

- [1] A.O. Sidorin et al., Nuclear Instr. Methods A 558, p. 325, 2006 (Joint Institute for Nuclear Research, Dubna, Russia <http://lepta.jinr.ru>).
- [2] C. Nieter, J. Cary, J. Comp. Phys. 196 , p.448 (2004); <http://www.txcorp.com>
- [3] S. Nagaitsev et al., PRL 96, 044801 (2006); <http://www-ecool.fnal.gov>
- [4] V.V. Parkhomchuk and I. Ben-Zvi, Tech. Report C-AD/AP/47 (2001).
- [5] V.V. Parkhomchuk, A.N. Skrinsky, Rep. Prog. Physics 54, p.919 (1991).
- [6] A.V. Fedotov et al., Proceedings of PAC05, p 4236; p.4251 (2005).
- [7] I. Ben-Zvi, AIP Conf. Proceedings 821 (COOL05, Galena, IL), p.75 (2005).
- [8] Ya. Derbenev, TJAB Note, February 2001 (unpublished).
- [9] V. Litvinenko, independently proposed to use undulator for recombination suppression (2005).
- [10] S. Chandrasekhar, *Principles of Stellar Dynamics* (U. Chicago Press, 1942).
- [11] Ya. Derbenev, A. Skrinsky, Part. Accelerators 8, p. 235 (1978).
- [12] J. J. Binney, MNRAS 181, p. 735 (1977).
- [13] D.L. Bruhwiler *et al.*, AIP Conf. Proceed. **773** (Bensheim, Germany, 2004), p. 394.
- [14] A. Fedotov, D. Bruhwiler, D. Abell A. Sidorin., AIP Conf. Proc. 821, p. 319 (2005).
- [15] A. Fedotov et al., Phys. Rev. ST Accel. Beams, V. 9, 074401 (2006)..
- [16] L. Prost et al., Workshop HB2006 (KEK, Tsukuba, Japan) (2006).
- [17] G. Bell et al., Presentation at RHIC electron cooling workshop (Upton, NY, May 2006).
- [18] A. Piwinski, Proc. of 9th Intern. Conf. High Energy Acc. (1974); CERN 92-01, p. 405.
- [19] M. Martini, CERN PS/84-9 (AA), 1984.
- [20] J. Bjorken and S. Mtingwa, Particle Accel. 13 (1983), p.115.
- [21] V. Lebedev, AIP Conf. Proc. 773 (HB2004), p. 440.
- [22] W. Fischer et al. Proceedings of EPAC02, p. 236 (2002).
- [23] J. Wei et al., AIP Conf. Proc. 773 (HB2004), p. 389.
- [24] A. Fedotov et al, unpublished (2004).
- [25] A. Fedotov et al, Workshop HB2006 (KEK, Tsukuba, Japan), 2006.
- [26] A. Burov, “Electron cooling against IBS”, FNL-TM-2258 (2003).
- [27] A. Fedotov et al., Proceedings of PAC05, p. 4263 (2005).
- [28] G. Parzen, Tech. Notes C-AD/AP/144, C-AD/AP/150 (2004).
- [29] M. Horndl et al., PRL 95, 243201 (2005).
- [30] A. Wolf, H. Danared, I. Kaganovich (private communications, 2006).
- [31] “eRHIC Zeroth-Order Design Report”, BNL C-A/AP Note 142 (2004)
http://www.agsrhichome.bnl.gov/eRHIC/eRHIC_ZDR.htm
- [32] N. Malitsky, R. Talman, “Unified Accelerator Libraries”, AIP 391 (1996).
- [33] S.A. Kheifets, B. Zotter, CERN Report CERN SL-95-92 (1995).
- [34] E. Pozdeyev, “Effects of electron beam charge-per-bunch ripple”, “Effect of trapped ions” (2006), to be written.
- [35] E. Pozdeyev, “Effects of beam-pipe wakes on electron beam” (October 2006).
- [36] V.V. Parkhomchuck, V.B. Reva, J. of Exp. and Theor. Physics, V.91, p. 975 (2000).
- [37] P.R. Zenkevich, A.E. Bolshakov, NIM A 441, p. 441 (2000).
- [38] V.B. Reva, Presentation at RHIC electron cooling workshop (Upton, NY, May 2006).
- [39] G. Wang, “Collective electron-ion interactions for RHIC e-cooler” (2006):
<http://www.bnl.gov/cad/ecooling>
- [40] I. Meshkov, S. Nagaitsev, J. Dietrich (private communication, 2006).